Channel coupling in $A(\vec{e},e'\vec{N})B$ reactions

James J. Kelly

Department of Physics, University of Maryland, College Park, Maryland 20742
(Received 1 October 1998; revised manuscript received 23 February 1999)

The sensitivity of momentum distributions, recoil polarization observables, and response functions for nucleon knockout by polarized electron scattering to channel coupling in final-state interactions is investigated using a model in which both the distorting and the coupling potentials are constructed by folding density-dependent nucleon-nucleon effective interactions with nuclear transition densities. Elastic reorientation, inelastic scattering, and charge exchange are included for all possible couplings within the model space. Calculations for ^{16}O are presented for 200 and 433 MeV ejectile energies, corresponding to proposed experiments at MAMI and TJNAF, and for ^{12}C at 70 and 270 MeV, corresponding to experiments at NIKHEF and MIT-Bates. The relative importance of charge exchange decreases as the ejectile energy increases, but remains significant for 200 MeV. Both proton and neutron knockout cross sections for large recoil momenta, $p_m > 300$ MeV/c, are substantially affected by inelastic couplings even at 433 MeV. Significant effects on the cross section for neutron knockout are also predicted at smaller recoil momenta, especially for low energies. Many of the response functions and polarization observables for nucleon knockout are quite sensitive to the coupling scheme, especially those which vanish in the absence of final-state interactions. Polarization transfer for proton knockout is insensitive to channel coupling, even for fairly low ejectile energies, but polarization transfer for neutron knockout retains non-negligible sensitivity to channel coupling for energies up to about 200 MeV. The present results suggest that possible medium modifications of neutron and proton electromagnetic form factors for $Q^2 \gtrsim 0.5$ (GeV/c)^2 can be studied using recoil polarization with relatively little uncertainty due to final-state interactions. [S0556-2813(99)01806-3]

PACS number(s): 25.30.Dh, 24.10.Eq, 24.70.+s, 27.20.+n

I. INTRODUCTION

Proton knockout by electron scattering has become established as the most accurate method for measuring recoil momentum distributions for nuclear single-hole states. With the high resolution available at NIKHEF, precise measurements of distorted momentum distributions have been made for discrete states in many nuclei [1]. Recent reviews of nucleon electromagnetic knockout reactions can be found in Refs. [2–4]. These studies have provided much information on the fragmentation of single-particle strength among various hole states in the residual nucleus. Although the missing momentum distributions for strongly excited states generally agree quite well in shape with mean-field calculations, the total strength observed is systematically lower than the single-particle strength. The quenching of the single-particle strength is attributed to correlations which spread that strength over broad ranges of both energy and momentum. Therefore, evidence for these correlations has been sought in single-nucleon knockout with large missing momentum for which correlations might be expected to enhance the yield with respect to mean-field models. However, because inelastic scattering and charge exchange contributions to final-state interactions (FSI's) can also enhance the yield for large missing momentum, it becomes important to extend the treatment of FSI's beyond the usual optical-model approach.

Another of the central problems of nuclear physics is to determine the sensitivity of hadronic properties to the local baryonic density. For example, an early hypothesis motivated by the EMC effect was that the nucleon charge radius increases with density. More recently, the quark-meson cou-

pling (QMC) model has been used to study the density dependence of the nucleon electromagnetic form factors [5–7] induced by coupling of their constituent quarks to the strong scalar and vector fields within nuclei. However, because the effects predicted are relatively small at normal nuclear densities, it will be very difficult to extract unambiguous results from measurements of cross sections for single-nucleon knockout from nuclei. Fortunately, recoil polarization observables are expected to be much less vulnerable than cross sections to uncertainties in spectral functions, gauge ambiguities, and off-shell extrapolation of the single-nucleon current operator [8]. In the one-photon-exchange approximation, the ratio between the longitudinal and coplanar transverse polarization transfers, P'_L/P'_S, is proportional to the ratio between electric and magnetic form factors, G_E/G_M, and this relationship is relatively insensitive to distortion by the optical potential for the ejectile. The primary objective of the present investigation is to determine the effect of channel coupling in final-state interactions, especially of charge exchange, upon recoil polarization.

Ideally one should evaluate the nuclear electromagnetic current using a many-body Hamiltonian which accurately describes both bound and scattering states. Calculations for ^{16}O$(e,e'N)$ have been performed for $T_N \approx 70$–100 MeV by Ryckebusch *et al.* [9] using a Hartree-Fock (HF) random phase approximation (RPA) model based upon a Skyrme interaction [10]. The roles of channel coupling and two-body currents at large missing momentum have also been investigated recently for $T_N \approx 100$ MeV by van der Sluys *et al.* [11]. Both bound and continuum wave functions are generated within the HF mean field for the Skyrme interaction.

The current operator is also based upon the HF Hamiltonian. Thus, this approach preserves gauge invariance and avoids orthogonality defects. On the other hand, because the mean field is real, attenuation of the scattered flux must be described by explicit coupling to the open channels. Coupling to all single-nucleon emission channels is included within the RPA, but more complicated configurations are omitted. Hence, although this model is internally consistent, its description of the final state interactions is limited to low ejectile energies and is not suitable for the upcoming experiments at MAMI and TJNAF.

Jeschonnek et al. [12] use a continuum RPA model in which coupling between single-nucleon emission channels is treated microscopically while coupling to more complicated channels is approximated using a phenomenological optical model. Coupling potentials were constructed using either a bound-state G matrix based upon the Bonn potential [13] or the Franey-Love parametrization of the t matrix [14]. Although this approach provides a more realistic model of absorption, it is now well established that the nucleon-nucleon effective interaction is strongly density dependent and cannot be accurately represented by a t matrix; nor is the bound-state G matrix appropriate for higher ejectile energies.

The local density approximation (LDA) based upon density-dependent empirical effective interactions (EEI's) does provide accurate fits to proton elastic, inelastic, and charge-exchange scattering for energies above 100 MeV [15–18]. The density dependence of effective interactions constructed for infinite nuclear matter, usually with G-matrix formalisms, is parametrized and the parameters are adjusted to fit proton elastic and inelastic scattering data for self-conjugate targets using states whose transition densities are measured by electron scattering. Both the distorting and the scattering potentials are based upon the same effective interaction, which is fitted using a self-consistency procedure. Sensitivity to the density dependence of the effective interaction is provided by use of both interior-peaked and surface-peaked transition densities. It has been shown that the empirical effective interaction is essentially independent of both state and target and that interactions fitted to inelastic scattering data provide good fits to elastic scattering whether or not those data are included in the analysis [19,16]. The EEI model also provides accurate predictions for proton absorption and neutron total cross section data [20]. Unlike optical-model analyses of elastic scattering data, which are sensitive only to the asymptotic properties of the wave function, represented by phase shifts, the overlap with interior-peaked transition densities gives the EEI analysis of inelastic scattering data sensitivity to the interior wave function. Finally, it has been shown that the EEI model accurately describes proton scattering data for ^{9}Be, where channel coupling within the rotational band plays an important role [21], even though the interactions were fitted to data for $A \geqslant 16$. Therefore, we believe that the local density approximation based upon empirical effective interactions should provide a superior description of FSI's for $A(\vec{e},e'\vec{N})B$ reactions at energies above 100 MeV.

We have developed a coupled-channel model for $A(\vec{e},e'\vec{N})B$ reactions which includes elastic reorientation, inelastic scattering, and charge exchange in FSI's based upon density-dependent effective interactions within the local den-

sity approximation. A simpler version of the model was used recently to analyze coupled-channel effects upon the distorted momentum distributions for the ^{10}B$(e,e'p)^9$Be and ^{10}B$(\gamma,p)^9$Be reactions [22]. Coupling within the ^{9}Be rotational band was evaluated using density-dependent nucleon-nucleon interactions folded with transition densities fitted to electron and proton scattering measurements. For missing momenta greater than 300 MeV/c quadrupole coupling is found to enhance the momentum distributions for $(e,e'p)$ in quasiperpendicular kinematics by factors up to 3–5 for various states; even larger effects are predicted for (γ,p). The model has since been extended to include charge-exchange coupling and to produce response functions and polarization observables. Some preliminary results were shown in Refs. [2,23].

In this paper we investigate the sensitivity of momentum distributions, response functions, and recoil polarization observables for $(\vec{e},e'\vec{N})$ reactions to both inelastic and charge exchange couplings in final-state interactions, emphasizing upcoming experiments that include recoil polarization. Experiments A1/2-93 at MAMI [24] and 89-033 at TJNAF [25] will look for modifications of the helicity-dependent recoil polarization in the ^{16}O$(\vec{e},e'\vec{p})$ reaction for $T_p \approx 200$ MeV and 433 MeV, respectively. In addition, experiment 89-003 at TJNAF will measure large missing momenta and will separate R_{LT} for ^{16}O$(e,e'p)$ for $T_p \approx 433$ MeV. Therefore, in this paper we investigate the effects of coupling between valence single-hole states in the ^{16}O$(\vec{e},e'\vec{N})$ reaction. Section II presents the coupled-channel formalism, Sec. III gives further details of the coupling potentials, and Sec. IV describes the observables and response functions for single-nucleon knockout. Results for representative cases are presented in Secs. V and VI. Our conclusions are summarized in Sec. VII.

II. COUPLED-CHANNEL FORMALISM FOR SINGLE-NUCLEON KNOCKOUT

A. Coupled equations for electron scattering

Suppose that the $e+A$ electronuclear system is described by a Hamiltonian of the form

$$\mathcal{H} = K_A + H_e + \mathcal{H}_A + V_{eA}, \tag{1}$$

where K_A is the kinetic energy of the nucleus, $H_e = -i\vec{\alpha} \cdot \vec{\nabla}_e + m_e\beta$ describes the motion of a free electron, $\mathcal{H}_A$ describes the internal dynamics of the nuclear system, and V_{eA} is the interaction between them. State vectors for the complete electronuclear system satisfy eigenvalue equations of the form $\mathcal{H}\Psi = E\Psi$, where E is the total energy. Let $\Psi_\alpha^{(+)}$ represent an electronuclear wave function that contains incoming Coulomb-distorted electron waves in channel α and outgoing waves in all open channels. The electronuclear wave function can be factored according to

$$\Psi_\alpha^{(+)}(\mathbf{r}_e,\mathbf{r}_A) = \int d^3 p'_{A\alpha} g(\mathbf{p}_{A\alpha} - \mathbf{p}'_{A\alpha})$$

$$\times \exp(i\mathbf{p}'_{A\alpha} \cdot \mathbf{r}_A) \sum_\beta \xi_{\alpha\beta}^{(+)}(\mathbf{r}_e) \psi_{A\beta}^{(-)}, \tag{2}$$

where $\mathbf{p}_{A\alpha}$ and $\mathbf{r}_A$ are the momentum and position of the nuclear center of mass and $\xi_{\alpha\beta}^{(+)}(\mathbf{r}_e)$ represents the motion of the electron. It is convenient to normalize the target wave packet to unity at the asymptotic momentum, such that $g(0) = 1$. The state vectors $\psi_{A\beta}$ for the nuclear subsystem satisfy eigenvalue equations of the form $\mathcal{H}_A \psi_{A\beta} = m_{A\beta} \psi_{A\beta}$ where $m_{A\beta}$ is the invariant mass of the nuclear system in channel β. The summation over state labels β is interpreted as a sum over discrete and integral over continuum states. The bound states include both elastic and inelastic electron scattering, while the continuum states include single-nucleon knockout, two-nucleon emission, and more complicated reaction channels.

Rawitscher investigated the asymptotic behavior of coupled electronuclear wave functions using the method of steepest descent [26] and demonstrated that when the proper boundary conditions are applied to the continuum states of the nuclear subsystem, only outgoing waves that satisfy energy conservation survive. The wave function $\xi_{\alpha\beta}^{(+)}$ contains a Coulomb wave in channel α and outgoing spherical waves in all open channels. Label α usually refers to the ground state of the target nucleus, but later we will also require electronuclear wave functions containing a Coulomb-distorted electron wave impinging instead upon an excited state of the nuclear system; that excited state may be unbound and may contain one or more ejectiles. Consequently, the nuclear system is described by a wave function $\psi_{A\beta}^{(-)}$ that satisfies incoming boundary conditions. Suppose that channel β refers to a proton ejectile plus a bound state of the $B = A - 1$ nucleus. The wave function $\psi_{A\beta}^{(-)}$ would then contain a Coulomb-distorted nucleon wave in channel β and incoming spherical waves in all open channels (including both β and $\beta' \neq \beta$) and would be related by time reversal to the wave function $\psi_{A\beta}^{(+)}$ that describes proton scattering by state β of target B. Of course, one does not normally have access to scattering by excited states.

Introducing distorting potentials $U_{e\beta}(\mathbf{r}_e)$ and projecting out the nuclear state β, we obtain coupled equations for the electron wave function that have the form

$$(E_{e\beta} - H_e - U_{e\beta})\xi_{\alpha\beta} = \sum_\gamma (V_{e\beta\gamma} - U_{e\gamma}\delta_{\beta\gamma})\xi_{\alpha\gamma}, \quad (3)$$

where $E_{e\beta} = E - K_{A\beta} - m_{A\beta}$ is the electron center-of-mass energy for channel β and where the coupling potentials are

$$V_{e\beta\gamma} = \langle \psi_{A\beta} | V_{eA} | \psi_{A\gamma} \rangle. \quad (4)$$

The equations for bound and continuum states of the residual nuclear system are formally identical, provided that the summation and boundary conditions are interpreted properly. For bound nuclear states, we could minimize the residual elastic terms on the right-hand side of Eq. (3) by choosing

$$U_{e\beta}(\mathbf{r}_e) \approx \langle \psi_{A\beta} | V_{eA} | \psi_{A\beta} \rangle, \quad (5)$$

but this choice may not converge for unbound states. Nevertheless, recognizing that the dominant electron-nucleus interaction is due to the spherical part of the elastic Coulomb potential, one generally chooses $U_{e\beta}(\mathbf{r}_e)$ to be the Coulomb potential produced by the charge density of the nuclear

ground state and neglects the interaction between the electron and the ejectiles that might be present in channel β. Presumably the effects of more complicated residual elastic terms can be evaluated perturbatively, if necessary. Note that these elastic terms also include magnetic contributions and recoil corrections to the static Coulomb potential. Therefore, we define electron distorted waves as the solutions to the homogeneous equations, such that

$$(E_{e\alpha} - H_e - U_{e\alpha})\zeta_\alpha(\mathbf{r}_e) = 0, \quad (6)$$

where $U_{e\alpha}$ is approximated by the ground-state Coulomb potential.

The transition matrix for inelastic transitions between initial state α and final state β can now be expressed in the prior representation as

$$\mathcal{M}_{\beta\alpha} = \int d^3 r_e d^3 r_A \langle \Psi_\beta^{(-)}(\mathbf{r}_e, \mathbf{r}_A) | V_{eA} |$$
$$\times \exp(i\mathbf{p}_{A\alpha} \cdot \mathbf{r}_A) \zeta_\alpha^{(+)}(\mathbf{r}_e) \psi_{A\alpha}^{(-)} \rangle, \quad (7)$$

where

$$\Psi_\beta^{(-)}(\mathbf{r}_e, \mathbf{r}_A) = \int d^3 p'_{A\beta} g(\mathbf{p}_{A\beta} - \mathbf{p}'_{A\beta})$$
$$\times \exp(i\mathbf{p}'_{A\beta} \cdot \mathbf{r}_A) \sum_\gamma \xi_{\beta\gamma}^{(-)}(\mathbf{r}_e) \psi_{A\gamma}^{(-)} \quad (8)$$

is a complete, fully coupled, wave function containing outgoing Coulomb waves in channel β and incoming waves in all open channels. Therefore, we obtain a matrix element of the general form

$$\mathcal{M}_{\beta\alpha} = \int d^3 p'_{A\beta} g(\mathbf{p}_{A\beta} - \mathbf{p}'_{A\beta}) \int d^3 r_e d^3 r_A$$
$$\times \exp[i(\mathbf{p}_{A\alpha} - \mathbf{p}'_{A\beta}) \cdot \mathbf{r}_A] \sum_\gamma \mathcal{V}_{\beta\gamma\alpha}(\mathbf{r}_e, \mathbf{r}_A), \quad (9)$$

where

$$\mathcal{V}_{\beta\gamma\alpha}(\mathbf{r}_e, \mathbf{r}_A) = \langle \xi_{\beta\gamma}^{(-)}(\mathbf{r}_e) \psi_{A\gamma}^{(-)} | V_{eA} | \zeta_\alpha^{(+)}(\mathbf{r}_e) \psi_{A\alpha}^{(-)} \rangle \quad (10)$$

is an effective electron-scattering potential obtained by integration over all internal coordinates of the nuclear system. The transition matrix element contains the effects of channel coupling produced by both the nucleon-nucleus and the electron-nucleus interactions. The summation over the index γ includes nuclear states excited by final-state interactions between the electron and the nuclear system, but these dispersion corrections are subsequently neglected. Channel coupling between nuclear states excited by nucleon-nucleus final-state interactions will be developed in Sec. II D.

The expression derived by Rawitscher, Eq. (4.7) of Ref. [26], for the inhomogeneous driving terms for electron scattering is very similar to our Eqs. (9) and (10). The primary difference is that we include a target wave packet to facilitate later use of the effective momentum approximation to develop a practical approximation. Another superficial difference is that we employ the prior representation, and hence have the coupled electron wave function on the left-hand

side of the transition matrix element, whereas he uses the post representation in which the coupled electron wave function appears on the right-hand side of his Eq. (2.16). Hence, dispersion corrections appear as final-state interactions here and as initial-state interactions in Ref. [26], but these representations should be equivalent in the absence of subsequent approximations.

Electromagnetic coupling between low-lying bound states is often described as dispersion corrections. For example, Mercer [27] evaluated dispersion corrections due to coupling to inelastic excitations of the target in the $A(e,e')A'$ reaction and found those effects to be quite small. The present formalism also includes coupling of the electron to more complicated states of the nuclear system, including knockout channels, but evaluation of these subtle effects would be very difficult computationally and is omitted. A qualitative discussion of some of these issues has been given by Rawitscher [26]. In the present work, we study single-nucleon knockout under conditions where the distortion of the electron wave functions is relatively small, namely, high energies and light targets. Therefore, we will neglect channel coupling that could arise from the electron-nucleus interaction and employ a simple approximation for the electron wave functions, namely, the effective momentum approximation. In the next several sections we outline the approximations used to perform practical calculations for single-nucleon knockout under conditions where channel coupling by nuclear FSI's can be important.

B. Single-nucleon knockout

For the present application we consider only the one-body part of the nuclear electromagnetic current. Hence, we approximate the electromagnetic interaction by the single-nucleon contribution

$$
\begin{aligned}
V_{eA} &\approx e^2 \int d^3 r_N \hat{j}_\mu(\mathbf{r}_e) \frac{\exp(i\omega r_{eN})}{r_{eN}} \hat{J}^\mu(\mathbf{r}_{NA}) \\
&= e^2 \int d^3 r_N \int \frac{d^3 q'}{(2\pi)^3} \hat{j}_\mu \frac{\exp(-i\mathbf{q}'\cdot\mathbf{r}_{eN})}{Q'^2} \hat{J}^\mu, \quad (11)
\end{aligned}
$$

where $\hat{j}_\mu$ and $\hat{J}^\mu$ are the electron and nucleon current operators, $Q'^2 = q'^2 - \omega^2$ is the photon virtuality, $\mathbf{r}_{eN} = \mathbf{r}_e - \mathbf{r}_N$ is the separation between the electron and the ejectile, and $\mathbf{r}_{NA} = \mathbf{r}_N - \mathbf{r}_A$ is the ejectile position relative to the barycentric system. Substituting Eqs. (2) and (11) into Eq. (9), we find

$$
\begin{aligned}
\mathcal{M}_{\beta\alpha} &\approx \sum_\gamma \int \frac{d^3 q'}{(2\pi)^3} \frac{4\pi\alpha}{Q'^2} g^*(\mathbf{q}-\mathbf{q}') \\
&\times \mathcal{J}^e_{\beta\gamma\alpha}(-\mathbf{q}') \cdot \mathcal{J}^N_{\gamma\alpha}(\mathbf{q}'), \quad (12)
\end{aligned}
$$

where $\mathbf{q} = \mathbf{p}_{A\beta} - \mathbf{p}_{A\alpha}$ is the asymptotic momentum transfer. The matrix elements of the electron and nuclear currents are contracted, and the fine structure constant α should not to be confused with state labels. The electron and nuclear current matrix elements are

$$
\mathcal{J}^{e\mu}_{\beta\gamma\alpha}(\mathbf{q}) = \int d^3 r_e \exp(i\mathbf{q}\cdot\mathbf{r}_e) \langle \xi^{(-)}_{\beta\gamma}(\mathbf{r}_e) | \hat{j}^\mu(\mathbf{r}_e) | \zeta_\alpha(\mathbf{r}_e) \rangle,
$$
$$
(13a)
$$

$$
\mathcal{J}^{N\mu}_{\gamma\alpha}(\mathbf{q}) = \int d^3 r_{NA} \exp(i\mathbf{q}\cdot\mathbf{r}_{NA}) \langle \psi^{(-)}_{A\gamma} | \hat{J}^\mu(\mathbf{r}_{NA}) | \psi^{(-)}_{A\alpha} \rangle.
$$
$$
(13b)
$$

Recognizing that it will be more convenient to express the nucleon distorted waves and overlap functions relative to the residual nucleus B than to the barycentric system, we rescale the charge and current density operators using

$$
\hat{J}^\mu(\mathbf{r}_{NA}) = \left(\frac{m_A}{m_B}\right)^3 \hat{J}^\mu(\mathbf{r}_{NB}), \quad (14)
$$

where $\mathbf{r}_{NB} = \mathbf{r}_N - \mathbf{r}_B = (m_A/m_B)\mathbf{r}_{NA}$ is the ejectile position relative to the residual nucleus. The nuclear current then becomes

$$
\mathcal{J}^{N\mu}_{\gamma\alpha}(\mathbf{q}) = \int d^3 r_{NB} \exp(i\mathbf{q}\cdot\mathbf{r}_{NA}) \langle \psi^{(-)}_{A\gamma} | \hat{J}^\mu(\mathbf{r}_{NB}) | \psi^{(-)}_{A\alpha} \rangle.
$$
$$
(15)
$$

The appearance of r_{NA} in the exponential is a familiar recoil correction (e.g., see [28]).

For light targets and relatively small ejectile momenta, it may be necessary to include electromagnetic interactions in which the momentum is received by the residual nucleus while the observed nucleon is a spectator. These contributions, often called exchange terms, can be included using a straightforward extension of the results presented here, but are negligible for applications involving energetic nucleons. Two-body currents are more complicated and will not be considered in the present work.

C. Electron current

We expect the final-state interactions between the nucleon ejectile and the residual nucleus to dominate over multiple hard scattering of the electron; therefore, we neglect inelastic contributions to the electron distorted waves and approximate $\xi_{\beta\gamma} \approx \zeta_\beta \delta_{\beta\gamma}$. Furthermore, the principal effect of Coulomb distortion of the electron wave functions for high-energy beams and light targets can be described using the effective momentum approximation (EMA) [29,30]

$$
\zeta \approx \frac{\bar{k}_e}{k_e} \exp(i\bar{\mathbf{k}}_e \cdot \mathbf{r}) u(\bar{\mathbf{k}}_e), \quad (16)
$$

where $u(\bar{\mathbf{k}}_e)$ is a free Dirac spinor with spin variables and where the local momentum

$$
\bar{\mathbf{k}}_e = \mathbf{k}_e + f_Z \frac{\alpha Z}{R_Z} \hat{\mathbf{k}} \quad (17)
$$

is increased relative to the asymptotic wave number k_e by the action of the Coulomb potential [31]. Here $f_Z = 1.5$ corresponds to the electrostatic potential at the center of a uniformly charged sphere of radius R_Z. An improved version of the EMA proposed by Kim and Wright [32] should allow the

present formalism to be applied to heavier targets, but has not yet been implemented in the coupled-channel code.

Thus, the electron current is approximated by

$$\mathcal{J}_{\beta\gamma\alpha}^{e\mu}(\mathbf{q}) \approx \mathcal{J}_{\mathrm{eff}}^{e\mu}(\mathbf{q}_{\mathrm{eff}}) \delta(\mathbf{q} - \mathbf{q}_{\mathrm{eff}}) \delta_{\beta\gamma}, \qquad (18)$$

where

$$\mathcal{J}_{\mathrm{eff}}^{e\mu}(\mathbf{q}_{\mathrm{eff}}) = \frac{\bar{k}_i \bar{k}_f}{k_i k_f} \bar{u}(\bar{\mathbf{k}}_f) \gamma^\mu u(\bar{\mathbf{k}}_i). \qquad (19)$$

Finally, we assume that the wave packets vary sufficiently slowly with momentum that we can replace $g(\mathbf{q} - \mathbf{q}_{\mathrm{eff}})$ by unity; in any case, the shape of the wave packet can be extracted from the definition of the differential cross section. Therefore, the transition matrix element reduces in the effective momentum approximation to

$$\mathcal{M}_{\beta\alpha} \approx \frac{4\pi\alpha}{Q_{\mathrm{eff}}^2} \mathcal{J}_{\mathrm{eff}}^e(-\mathbf{q}_{\mathrm{eff}}) \cdot \mathcal{J}_{\beta\alpha}^N(\mathbf{q}_{\mathrm{eff}}), \qquad (20)$$

where $Q_{\mathrm{eff}}^2 = \mathbf{q}_{\mathrm{eff}}^2 - \omega^2$ and where the nuclear current, given by Eq. (13), includes channel coupling by the nuclear final-state interactions.

D. Coupled equations for nuclear FSI's

Suppose that the residual nucleon-nucleus system is described by a Hamiltonian of the form

$$\mathcal{H}_A = m_N + K_{NB} + H_B + V_{NB}, \qquad (21)$$

where K_{NB} is the kinetic energy operator for relative motion, H_B is the internal Hamiltonian of the residual nucleus, and V_{NB} is the potential energy for the nucleon-nucleus interaction and is real. We also include the ejectile mass m_N, but neglect its possible internal excitations. The orthonormal state vectors of the residual nucleus satisfy eigenvalue equations of the form

$$H_B \Phi_\beta = m_{B\beta} \Phi_\beta, \qquad (22)$$

where $m_{B\beta}$ is the invariant mass of the residual nucleus in channel β. Recognizing that it is impractical to retain the complete set of eigenstates for the nuclear system, it is useful to introduce the model-space projection operators P and Q, where P selects the states of interest (the model space) and $Q = 1 - P$ selects the rest (excluded space) such that $P^2 = P$, $Q^2 = Q$, and $PQ = QP = 0$. One would normally limit the model space to a set of states that are strongly populated by the direct reaction $A(e,e'N)B$, here valence states reached by single-nucleon knockout, plus other states of interest that can be reached by final-state interactions, here $B(N,N')B'$.

Using standard manipulations (e.g., Ref. [33]), it is straightforward to show that projected state vectors within the model space satisfy eigenvalue equations of the form

$$(m_{A\alpha} - H_{\mathrm{eff}}) P \psi_\alpha^{(+)} = 0, \qquad (23)$$

where the effective Hamiltonian for the model space,

$$H_{\mathrm{eff}} = H_{PP} + H_{PQ}(m_{A\alpha}^+ - H_{QQ})^{-1} H_{QP}, \qquad (24)$$

includes the effects of the excluded space and where $m_{A\alpha}^+ = m_{A\alpha} + i\delta$ includes a positive infinitesimal δ to ensure outgoing boundary conditions. We use the customary notation $C\mathcal{H}_A D = H_{CD}$, where $C,D \in \{P,Q\}$. The effective Hamiltonian depends upon the model space selected and is complex, energy dependent, nonlocal, and far too complicated for practical applications. Therefore, it is customary to approximate the effective model-space Hamiltonian by

$$\mathcal{H}_{\mathrm{eff}} \approx m_N + K_{NB} + H_B + U, \qquad (25)$$

where U is a complex effective interaction. Although the formalism applies equally well to nonlocal effective interactions, we will employ local approximations in our applications. For elastic channels U is identified with the optical potential, whereas for inelastic channels U becomes a transition potential. Although one often employs phenomenological optical potentials fitted to elastic scattering data, we prefer to use microscopic potentials for both elastic and inelastic scattering obtained by folding density-dependent effective interactions with nuclear transition densities.

Thus, we can expand the model-space wave functions according to

$$P\psi_{A\gamma}^{(+)} = \sum_\eta \chi_{\gamma\eta}^{(+)}(\mathbf{r}_{NB}) \Phi_\eta, \qquad (26)$$

where the Φ_η are state vectors of the residual nucleus and $\chi_{\gamma\eta}^{(+)}(\mathbf{r}_{NB})$ is the coupled-channel wave function for relative motion containing incoming waves in channel γ and outgoing waves in all states within the model space. Separating the dominant distorting potentials from the smaller coupling terms, we now find that the channel wave functions satisfy coupled equations of the form

$$(m_{A\gamma} - m_{B\eta} - m_{N\eta} - K_{NB} - U_\eta)\chi_{\gamma\eta} = \sum_\kappa' U_{\eta\kappa}\chi_{\gamma\kappa}, \qquad (27)$$

where $U_{\eta\kappa}$ are the coupling potentials and where U_η contains the central and spin-orbit components of the elastic potential for channel η. One could include the complete elastic potential on the left, but it is computationally more convenient to place the small nonspherical parts of the elastic potential (if any) on the right. The primed summation indicates that any elastic terms included on the left are excluded from the right.

We have decided for the present applications to express the coupled equations in the form of relativized Schrödinger equations. Although there exists no rigorous justification for this procedure, it is common in analyses of nucleon-nucleus scattering to employ a prescription which replaces the center-of-mass kinetic energy and its corresponding operator by

$$m_{A\gamma} - m_{B\eta} - m_{N\eta} \rightarrow \frac{k_\eta^2}{2\mu_\eta}, \qquad (28a)$$

$$K_{NB} \rightarrow \frac{-\nabla_{NB}^2}{2\mu_\eta}, \qquad (28b)$$

where k_η is the exact relativistic wave number in the NB system and μ_η is the relativistic reduced energy for channel η. This procedure gives the correct de Broglie wavelength and reproduces the correct relativistic density of states [34]. The coupled equations are then expressed in coordinate space as

$$(\nabla^2 + k_\eta^2 - 2\mu_\eta U_\eta)\chi_{\gamma\eta} = 2\mu_\eta \sum_\kappa{}' U_{\eta\kappa}\chi_{\gamma\kappa}. \qquad (29)$$

Alternatively, one could describe nucleon-nucleus final-state interactions using the Dirac equation by means of the replacement

$$m_N + K_{NB} + U \to -i\vec{\alpha}\cdot\vec{\nabla}_{NB} + \beta(m_N + S) + V, \qquad (30)$$

where S and V are Dirac scalar and vector potentials; additional Dirac potentials may be present also. However, this approach requires a relativistic treatment of the nuclear structure and the inelastic scattering potentials, which is generally more difficult than the relativized Schrödinger approach. Although several Dirac coupled-channel calculations for proton-nucleus scattering have been performed using coupling potentials based upon the collective model [35,36], we are interested in charge-exchange and single-particle transitions which require a more microscopic treatment of the coupling potentials. Fortunately, it has been shown that nucleon-nucleon interactions for the relativistic impulse approximation can be represented in terms of equivalent density-dependent effective interactions suitable for use in the relativized Schrödinger formalism [37,38]. Furthermore, there exist empirical effective interactions fitted to nucleon-nucleus elastic and inelastic scattering data over a wide range of energies. Therefore, we chose to employ the relativized Schrödinger approach, which is computationally simpler than coupled Dirac equations, with scattering potentials based upon the impulse approximation.

E. Effective current operator

It is also important to recognize that use of an effective Hamiltonian should be accompanied by renormalization of the current operator [39]. The requirement that model-space matrix elements of the effective current operator $\hat{J}^\mu_{\text{eff}}$ reproduce those of the bare current operator $\hat{J}^\mu$ acting on complete wave functions is expressed by the condition

$$\langle\psi_{A\gamma}|\hat{J}^\mu|\psi_{A\alpha}\rangle = \langle\psi_{A\gamma}|P\hat{J}^\mu_{\text{eff}}P|\psi_{A\alpha}\rangle. \qquad (31)$$

Thus, one obtains the formal expression

$$\begin{aligned}
\hat{J}^\mu_{\text{eff}} = \hat{J}^\mu_{PP} &+ \hat{J}^\mu_{PQ}(E^+ - H_{QQ})^{-1}H_{QP} \\
&+ H_{PQ}(E^+ + \omega - H_{QQ})^{-1}\hat{J}^\mu_{QP} \\
&+ H_{PQ}(E^+ + \omega - H_{QQ})^{-1}\hat{J}^\mu(E^+ - H_{QQ})^{-1}H_{QP},
\end{aligned}$$
$$(32)$$

where E is the energy of the initial state and $E + \omega$ is the energy of the final state. This expression was obtained first by Boffi *et al.* [39], who further assumed that $\hat{J}^\mu_{PQ} = \hat{J}^\mu_{QP}$

=0. An alternative expression for the effective current operator in terms of the Green's function for the coupled equations has been given by Rawitscher [26]. However, these expressions are extremely complicated and have never been evaluated for realistic nuclear models. Hence, we conform with the universal and usually implicit practice of assuming without proof that $\hat{J}_{\text{eff}} \approx \hat{J}$.

Furthermore, in the spirit of the effective momentum approximation, we replace momentum operators appearing in the nuclear current operator by their asymptotic values. This approximation is consistent with the level of other approximations implicit in the replacement of the effective current with an off-shell current operator based upon the free single-nucleon current. Moreover, this procedure greatly simplifies the evaluation of the transition matrix elements, with the electromagnetic vertex function reducing to a matrix acting upon nucleon spin. Although it would be straightforward to evaluate the momentum operators completely, the inherent ambiguities in the choice of current operator [8] do not justify the computational cost.

Finally, note that by reducing the effective current operator to a two-dimensional matrix acting on nucleon spins, the effective momentum approximation permits the nucleon current operator to be evaluated in the laboratory frame even though the distorted wave calculations are performed in the barycentric frame. Hence, the current matrix elements in Eq. (13) and the corresponding electromagnetic response tensors are both evaluated in the laboratory frame.

We used the Γ_{cc1} off-shell vertex function of de Forest [40] with nucleon form factors from model 3 of Gari and Krümpelmann [41,42]. Current conservation was enforced at the one-body level by modifying the longitudinal component of the current, which is equivalent to evaluating the Feynman matrix element in the Coulomb gauge. However, significant ambiguities persist in the off-shell behavior of the nucleon electromagnetic vertex operator, which have been investigated by many authors, e.g., [40,43–46], without a clear resolution. We studied the consequences of these ambiguities for recoil polarization in the $A(\vec{e},e'\vec{N})$ reaction under conditions of interest to experiments presently being performed at MAMI and TJNAF [8]. Nevertheless, we expect that the qualitative changes relative to standard optical model distortion that are produced by couplings to specific final states will be largely independent of these ambiguities.

F. Nuclear current

We now specialize to the case where the initial state contains the ground state of the target, and denote the nuclear current for excitation of state β as $\mathcal{J}^{N\mu}_\beta = \mathcal{J}^{N\mu}_{\beta 0}$ and the corresponding transition matrix element as $\mathcal{M}_\beta = \mathcal{M}_{\beta 0}$. Given that the nuclear electromagnetic current operator has been approximated by a one-body operator, it is now appropriate to make a parentage expansion for the ground state of the target, such that

$$P\psi_0(\mathbf{r}_{NB}) = \sum_{\lambda\nu} c_{\lambda\nu}\phi_{\lambda\nu}(\mathbf{r}_{NB})\Phi_\lambda, \qquad (33)$$

where $c_{\lambda\nu}$ is a parentage coefficient (or pickup amplitude) and $\phi_{\lambda\nu}(\mathbf{r}_{NB})$ is an overlap function which describes the

amplitude for removing a nucleon with single-particle quantum numbers ν at position $\mathbf{r}_{NB}$ relative to the core and leaving the residual nucleus in state Φ_λ. The overlap function

$$\phi_{\lambda\nu}(\mathbf{r}) = R_{\lambda\nu}(r) \sum_{m_l, m_j} \left\langle \begin{array}{cc} l_\nu & \frac{1}{2} \\ m_l & m_j - m_l \end{array} \middle| \begin{array}{c} j_\nu \\ m_j \end{array} \right\rangle$$
$$\times \left\langle \begin{array}{cc} j_\nu & I_\lambda \\ m_j & m_\lambda \end{array} \middle| \begin{array}{c} I_0 \\ m_0 \end{array} \right\rangle Y_{l_\nu m_l}(\hat{r}) \chi_{m_j - m_l} \qquad (34)$$

includes a radial function and the usual coupling of spherical harmonics and nucleon spinors to the spin of the residual nucleus, I_λ, to produce the target spin I_0. The angular brackets denote Clebsch-Gordon coefficients. The parentage coefficient $c_{\lambda\nu}$ requires two indices whenever $I_0 \neq 0$. By extending the procedures outlined in Sec. II D, one could in principle develop a set of coupled equations governing the overlap functions [47]. However, one expects $\phi_{\lambda\nu}(\mathbf{r}_{NB})$ to resemble a bound-state wave function in the potential generated by the residual nucleus. Furthermore, analyses of $(e,e'p)$ data produce phenomenological overlap functions which are consistent in shape with single-particle wave functions based upon mean-field (Hartree-Fock) calculations. Hence, we employ either Hartree-Fock wave functions or Woods-Saxon wave functions fitted to $(e,e'p)$ data. More refined calculations in the future could employ overlap functions projected from correlated wave functions.

Substituting the parentage expansion, the nuclear current now becomes

$$\mathcal{J}_\beta^{N\mu}(\mathbf{q}_{\text{eff}}) \approx \sum_{\lambda\nu} c_{\lambda\nu} \int d^3 r_{NB} \exp(i\mathbf{q}_{\text{eff}} \cdot \mathbf{r}_{NA})$$
$$\times \langle \chi_{\beta\lambda}^{(-)}(\mathbf{r}_{NB}) | \hat{j}_{\text{eff}}^\mu(\mathbf{r}_{NB}) | \phi_{\lambda\nu}(\mathbf{r}_{NB}) \rangle. \qquad (35)$$

Finally, using the effective momentum approximation for the nucleon current operator, we obtain

$$\mathcal{J}_\beta^{N\mu}(\mathbf{q}_{\text{eff}}) \approx \sum_{\lambda\nu} c_{\lambda\nu} \int d^3 r_{NB} \ \exp(i\mathbf{q}_{\text{eff}} \cdot \mathbf{r}_{NA})$$
$$\times \langle \chi_{\beta\lambda}^{(-)}(\mathbf{r}_{NB}) | \hat{j}_{\text{eff}}^\mu(\mathbf{p}_{m,\text{eff}} + \mathbf{q}_{\text{eff}}, \mathbf{p}_{m,\text{eff}}) |$$
$$\times \phi_{\lambda\nu}(\mathbf{r}_{NB}) \rangle, \qquad (36)$$

where $\mathbf{p}_{m,\text{eff}} = \mathbf{p}_{N\beta} - \mathbf{q}_{\text{eff}}$ is the missing momentum determined by the ejectile momentum $\mathbf{p}_{N\beta}$ and the effective momentum transfer $\mathbf{q}_{\text{eff}}$. Thus, the nucleon current operator $\hat{j}_{\text{eff}}^\mu(\mathbf{p}_{m,\text{eff}} + \mathbf{q}_{\text{eff}}, \mathbf{p}_{m,\text{eff}})$ has been reduced to a matrix that acts upon nucleon spin.

This is the central result of the effective-momentum approximation to the coupled-channel formalism for FSI's in nucleon knockout by electron scattering. A similar electro-excitation amplitude was proposed by Blok and van der Steenhoven [48] based upon more qualitative arguments that exploit the similarity between knockout and pickup reactions. The primary difference between this expression and the standard distorted-wave approximation (DWA) is that the coupled-channel wave function replaces the usual distorted wave. Thus, we recover the DWA by neglecting the FSI coupling potentials, such that $\chi_{\beta\lambda} \rightarrow \chi_{\beta\lambda}^{(0)} \delta_{\beta\lambda}$. Also note that

for single-nucleon knockout from a spinless target, one generally assumes that the overlap function is well approximated by a unique single-particle wave function, such that $c_{\lambda\nu} \rightarrow \sqrt{S_\lambda} \delta_{\lambda\nu}$, where S_λ is the spectroscopic factor. However, the coupled-channel approach is much more general. For example, states for which the single-nucleon parentage coefficients are vanishingly small can still be populated by final-state interactions following an intermediate step that involves a state that is strongly excited by single-nucleon knockout [48,2,26].

III. FINAL-STATE INTERACTIONS

A. Partial-wave potentials

For each pair of channels (with suppressed labels), the scattering operator can be decomposed into a sum of products

$$U = \sum_{\kappa\lambda} \nu_{\kappa\lambda}(r) \mathcal{P}_{\kappa\lambda} \cdot \mathcal{T}_{\kappa\lambda}, \qquad (37)$$

in which $\nu_{\kappa\lambda}(r)$ contains the dependence upon relative separation and where the multipole operators $\mathcal{P}_{\kappa\lambda}$ and $\mathcal{T}_{\kappa\lambda}$ depend only on the angular momenta and internal variables of the projectile and target, respectively. The angular momentum transfer is designated λ, whereas κ is used to distinguish between different operators with the same multipolarity. Partial-wave potentials of the form

$$U_{\beta\gamma J} = \langle l_\beta s_\beta j_\beta I_\beta JM | U | l_\gamma s_\gamma j_\gamma I_\gamma JM \rangle \qquad (38)$$

then become

$$U_{\beta\gamma J} = \sum_{\kappa\lambda} \Gamma_{\lambda J}(j_\beta I_\beta; j_\gamma I_\gamma) \nu_{\beta\gamma\kappa\lambda}, \qquad (39)$$

where the recoupling coefficient is

$$\Gamma_{\lambda J}(j_\beta I_\beta; j_\gamma I_\gamma) = (-)^{j_\gamma + I_\beta + J} \hat{j}_\beta \hat{I}_\beta \begin{Bmatrix} j_\beta & j_\gamma & \lambda \\ I_\gamma & I_\beta & J \end{Bmatrix} \qquad (40)$$

and where

$$\nu_{\beta\gamma\kappa\lambda}(r) = \nu_{\kappa\lambda}(r) \langle l_\beta s_\beta j_\beta \| \mathcal{P}_{\kappa\lambda} \| l_\gamma s_\gamma j_\gamma \rangle \langle \beta I_\beta \| \mathcal{T}_{\kappa\lambda} \| \gamma I_\gamma \rangle \qquad (41)$$

are the appropriate multipole potentials, including angular and target matrix elements. The orbital angular momentum l_β is combined with the projectile spin s_β to give $\mathbf{j}_\beta = \mathbf{l}_\beta + \mathbf{s}_\beta$, which is then coupled to the target spin I_β to give the channel spin $\mathbf{J} = \mathbf{I}_\beta + \mathbf{j}_\beta$. Also note that $\hat{j} = \sqrt{2j+1}$ for angular momenta. A standard partial wave analysis of the coupled equations is made and the equations for each channel spin are solved by an iterative technique based upon that of Raynal [49].

The coupling potentials that would emerge from Eqs. (24) and (25) depend upon the chosen model space and are complex, nonlocal, energy-dependent, and otherwise intractable for practical applications. However, when the model space is a very small fraction of the available phase space, the dependence of the effective Hamiltonian upon the selection of states should be negligible. Furthermore, for energetic nucle-

ons and low-lying nuclear excitations, it is reasonable to approximate the coupling potentials using the impulse approximation based upon a density-dependent nucleon-nucleon interaction that provides good descriptions of nucleon elastic, inelastic, and charge-exchange scattering to similar states. Therefore, we constructed both optical and coupling potentials by folding a local density-dependent nucleon-nucleon interaction with nuclear transition densities that describe the relevant aspects of the target structure. Details of the implementation of the folding model may be found in Ref. [50].

It has been shown that the isoscalar spin-independent central, t_{00}^C, and isoscalar spin-orbit, t_0^{LS}, components of the effective interaction depend strongly upon local density [51], but are essentially independent of target [16]. However, although nuclear matter theory provides a good qualitative description of these effects, theoretical interactions are not yet sufficiently accurate [52,15]. Therefore, for energies above 100 MeV we employ the empirical effective interactions fitted to proton elastic and inelastic scattering data that are tabulated in Ref. [38], performing interpolations with respect to energy when needed. For lower energies we use the density-dependent Paris-Melbourne effective interaction [53,54]. All components of the effective interaction except tensor exchange were included in the coupled-channel calculations. The isoscalar components of coupling potentials include the Cheon rearrangement factor [55,56], which has been shown to be essential to the consistency between elastic and inelastic scattering in the analysis of the empirical effective interaction [15]. Rearrangement corrections for isovector interactions are more complicated but less important [57] and are omitted.

B. Model space

Each state in the model space can be populated by direct single-nucleon knockout or by final-state interactions following excitation of another member of the model space. All possible couplings between members of the model space are included. For a model space with n states there will be $n(n+1)/2$ couplings between states, each with several possible multipolarities depending upon the spins involved. For each multipolarity, there will be several potentials based upon various components of the nucleon-nucleon effective interaction.

It is useful to distinguish between four types of coupling mechanisms. Coupling potentials which do not change the state of the residual nucleus but which are omitted from the distorting (optical) potentials are classified as *elastic reorientation*; reorientation effects are often dominated by quadrupole potentials, when possible, but also include other allowed multipolarities. *Inelastic excitations* change the state of the residual nucleus without changing its charge; because the residual nucleus often has nonzero spin, several multipolarities are usually possible. *Analog transitions* change the charge of the residual nucleus without changing its spin, and also include several multipolarities when the spin is greater than zero. Finally, *nonanalog charge-exchange* transitions change both the internal state and the charge of the residual nucleus.

The present formalism is sufficiently general to accommodate sophisticated structure models in which correlations spread the single-particle strength over many fragments and modify the radial overlap functions. Such correlations would also affect the one-body density matrix element (OBDME) used to construct coupling potentials between members of the model space. However, because the computational cost increases rapidly with the size of the model space, it is necessary to limit the model space to the states of interest and those to which coupling is strongest.

In the present paper we consider coupling between low-lying discrete states with strong direct knockout amplitudes, for which the most important effects of channel coupling are likely to be dominated by the strongest fragments. In an earlier paper [2] we had studied indirect excitation of states with negligible direct knockout amplitudes and demonstrated that under some conditions multistep processes dominate, thereby improving upon the two-step calculations of Blok and van der Steenhoven [48]. However, we have also demonstrated that states of this type are excited too weakly to affect states with strong direct amplitudes and may be safely omitted from the model space. Furthermore, we assume that the coupling of low-lying discrete states to continuum states of the residual nucleus is adequately represented through continuum contributions to the imaginary parts of the optical and coupling potentials and that continuum states need not be included explicitly in the model space. Finally, we assume for these exploratory calculations that the independent-particle model (IPM) provides an adequate representation of single-nucleon knockout summed over related fragments. Therefore, the calculations were performed using IPM parentage coefficients and comparisons to experimental data include spectroscopic factors to normalize the strengths of the observed fragments.

The IPM space for $^{12}C(e,e'N)$ consists of the $(1s_{1/2})^{-1}$ and $(1p_{3/2})^{-1}$ proton-hole states in ^{11}B reached by the $(e,e'p)$ reaction and the analog states in ^{11}C reached by the $(e,e'n)$ reaction, for a total of four states. In addition to these $(1s_{1/2})^{-1}$ and $(1p_{3/2})^{-1}$ hole states, the IPM space for $^{16}O(e,e'N)$ also includes the $(1p_{1/2})^{-1}$ hole states in ^{15}N and ^{15}O, for a total of six states. In the context of the IPM space, we speak of the $(1s_{1/2})^{-1}$ hole configuration as a discrete state even though its spreading width is actually appreciable. The underlying continuum of two-nucleon and multinucleon knockout states then constitute the excluded space whose effects upon the reaction would, in principle, be represented through their influence upon the effective Hamiltonian and effective current operators. However, in practice simple approximations to these effective operators are employed as described above.

The parentage coefficients for pure hole states are given by $c_{\beta\gamma}=\sqrt{2j_\gamma+1}$ where $j_\gamma=I_\beta$ is the spin of the residual nucleus. The OBDME for coupling between pure hole states are given by

$$\langle\beta^{-1}\|[a_p^\dagger\otimes a_h]_J\|\gamma^{-1}\rangle=\hat{j}_p\delta_{J,0}\delta_{ph}\delta_{\beta\gamma}$$

$$+(-)^{j_\gamma+j_\beta-J}\frac{\hat{J}}{\hat{J}_\beta}\delta_{p\gamma}\delta_{h\beta},$$

$$(42)$$

where the initial state is described as a hole in orbital γ and the final state as a hole in orbital β for an otherwise closed-

shell nucleus. We generally assume that the $(J=0,T=0)$ term is already included in the spherical optical potential, so that only the second term of Eq. (42) contributes to the coupling potentials.

Overlap functions were represented by Woods-Saxon single-particle wave functions and fitted to $(e,e'p)$ data where available. Very similar results are obtained using Hartree-Fock wave functions. Possible modifications of the radial wave functions by short-range correlations can be incorporated easily.

IV. OBSERVABLES AND RESPONSE FUNCTIONS FOR $A(\vec{e},e'\vec{N})B$

A. Observables

Nucleon knockout reactions of the type $A(\vec{e},e'\vec{N})B$ initiated by a longitudinally polarized electron beam and for which the ejectile polarization is detected may be described by a doubly differential cross section of the form [58,59]

$$\frac{d^5\sigma_{hs}}{d\varepsilon_f d\Omega_e d\Omega_N} = \sigma_0 \frac{1}{2}[1+\mathbf{P}\cdot\boldsymbol{\sigma}+h(A+\mathbf{P}'\cdot\boldsymbol{\sigma})], \quad (43)$$

where $\varepsilon_i(\varepsilon_f)$ is the initial (final) electron energy, σ_0 is the unpolarized cross section, h is the electron helicity, s indicates the nucleon spin projection upon $\boldsymbol{\sigma}$, $\mathbf{P}$ is the induced polarization, A is the electron analyzing power, and $\mathbf{P}'$ is the polarization transfer coefficient. Thus, the net polarization of the recoil nucleon $\boldsymbol{\Pi}$ has two contributions of the form

$$\boldsymbol{\Pi}=\mathbf{P}+h\mathbf{P}', \quad (44)$$

where $|h|\leq 1$ is interpreted as the longitudinal beam polarization.

The recoil polarization is usually calculated with respect to a helicity basis in the barycentric frame defined by the basis vectors

$$\hat{\mathbf{L}}=\frac{\mathbf{p}_N}{|\mathbf{p}_N|}, \quad (45a)$$

$$\hat{\mathbf{N}}=\frac{\mathbf{q}\otimes\hat{\mathbf{L}}}{|\mathbf{q}\otimes\hat{\mathbf{L}}|}, \quad (45b)$$

$$\hat{\mathbf{S}}=\hat{\mathbf{N}}\otimes\hat{\mathbf{L}}. \quad (45c)$$

However, since this basis is not well defined when $\mathbf{q}$ and $\mathbf{p}_N$ are either parallel or antiparallel, these cases are conventionally handled by first rotating the reaction plane to ϕ_N as it would be in nonparallel kinematics, and then taking the limit $\theta_{pq}\to 0°$ or $\theta_{pq}\to 180°$ as required. Note that since the basis vectors $\hat{\mathbf{S}}$ and $\hat{\mathbf{N}}$ reverse directions when $\phi\to\phi+\pi$, the corresponding components of the recoil polarizations also tend to reverse sign even when there is no physical asymmetry with respect to ϕ; this behavior is simply an artifact of the basis.

Alternatively, since the recoil polarization is measured in the laboratory frame, it is useful to employ a polarimeter basis in which

$$\hat{\mathbf{y}}=\frac{\mathbf{k}_i\otimes\mathbf{k}_f}{|\mathbf{k}_i\otimes\mathbf{k}_f|}, \quad (46a)$$

$$\hat{\mathbf{x}}=\frac{\hat{\mathbf{y}}\otimes\mathbf{p}_N}{|\hat{\mathbf{y}}\otimes\mathbf{p}_N|}, \quad (46b)$$

$$\hat{\mathbf{z}}=\hat{\mathbf{x}}\otimes\hat{\mathbf{y}}. \quad (46c)$$

One advantage of presenting the recoil polarization in the laboratory or polarimeter basis is that the recoil polarization components are continuous as $\mathbf{p}_N$ moves through $\mathbf{q}$ from one side to the other. Unlike $\hat{\mathbf{S}}$ and $\hat{\mathbf{N}}$, $\hat{\mathbf{x}}$ and $\hat{\mathbf{y}}$ do not reverse directions when $\phi\to\phi+\pi$. For coplanar quasiperpendicular kinematics with $\hat{\mathbf{y}}$ upwards, it has become conventional to assign positive missing momentum to ejectile momenta on the large-angle side of $\mathbf{q}$, such that $\phi=\pi$ and $\theta_{pq}>0$.

The distorted missing momentum distribution $\rho^D(\mathbf{p}_m,\mathbf{p}')$, which is more properly called the reduced cross section, is obtained by dividing the unpolarized differential cross section σ_0 by the elementary electron-nucleon cross section σ_{eN} for initial (final) nucleon momenta $\mathbf{p}_m(\mathbf{p}')$, such that

$$\rho^D(\mathbf{p}_m,\mathbf{p}')=\frac{\sigma_0}{K\sigma_{eN}}, \quad (47)$$

where

$$\sigma_{eN}=\frac{\varepsilon_f}{\varepsilon_i}\frac{\alpha^2}{Q^4}\eta_{\mu\nu}\mathcal{W}_{eN}^{\mu\nu} \quad (48)$$

is based upon the plane-wave impulse approximation (PWIA) response tensor for off-shell kinematics and does not include the phase-space factor K. To be consistent, the eN response tensor must be computed from the same current operator and gauge used to evaluate the nuclear response tensor. The normalization is determined by the requirement that in the plane-wave approximation the momentum distribution $\rho_j(p_m)$ for a fully occupied orbital with total angular momentum j be normalized to its occupancy, such that

$$4\pi\int dp_m p_m^2 \rho_j(p_m)=2j+1 \quad (49)$$

for the independent-particle shell model.

B. Response functions

Additional insight into the reaction mechanism can be obtained by examining response functions. In the one-photon-exchange approximation the observables may be represented in terms of sums of products between kinematical factors which depend only on electron scattering kinematics and response functions which represent the dynamical content of the reaction. The details of the response-function decomposition have been given many times before and will be omitted here—we employ the definitions and notation of Ref. [2].

However, distortion of the electron wave function perturbs the relationship between the asymptotic electron-scattering kinematics and the momentum transfer delivered by the hard virtual photon, thereby introducing additional

dependencies upon azimuthal angle ϕ and upon electron scattering kinematics. Nevertheless, these effects are small enough for high-energy electrons and light targets to usefully employ the response function decomposition. For our purposes it will be instructive and sufficient to display response functions obtained by neglecting electron distortion.

It is useful to distinguish between class I response functions that would remain finite in the absence of final-state interactions and class II response functions which would vanish if FSI's could be eliminated. Clearly one expects class II response functions to be more sensitive to the details of final-state interactions than class I. Class I includes the unpolarized R_L, R_T, R_{LT}, and R_{TT} response functions, $R_{LT}'^N$, and both $R_{LT}'^m$ and $R_{TT}'^m$ with $m \in \{L, S\}$. Class II includes R_{LT}', R_L^N, R_T^N, R_{LT}^N, R_{TT}^N, and both R_{LT}^m and R_{TT}^m with $m \in \{L, S\}$.

C. Kinematics

The invariant mass of the final nuclear system is given by $W^2 = m_A^2 + 2m_A\omega - Q^2$. For the purposes of describing the final-state interactions, it is useful to define T_0 to be the ejectile energy in the rest frame of the residual nucleus, such that $W^2 = (m_N + m_B)^2 + 2m_B T_0$. The value quoted for T_0 is evaluated for the ground state of the nucleus reached in the $(e, e'p)$ reaction. Solving for T_0, we obtain

$$T_0 = \frac{m_A}{m_B}\left[\omega - E_m - \frac{Q^2 + E_m^2}{2m_A}\right], \qquad (50)$$

where $E_m = m_N + m_B - m_A$ is the missing energy. Similarly, the missing momentum is defined by $\mathbf{p}_m = \mathbf{p}_N - \mathbf{q}$.

For each missing momentum distribution, we hold W, or equivalently T_0, constant so that FSI's can be computed for a unique total energy. To minimize variations in electron distortion, the beam energy is also fixed. Parallel kinematics are defined by the subsidiary condition $\theta_{pq} = 0$ and $p_m = p_N - q$ is varied by adjusting both ω and $\mathbf{q}$ as required to maintain both $\theta_{pq} = 0$ and constant T_0. Quasiperpendicular kinematics maintain constant $(\omega, \mathbf{q})$ and require $p_m = 0$ for the $(e, e'p)$ ground-state transition when $\theta_{pq} = 0$. The missing momentum is varied by changing θ_{pq} and is conventionally defined as positive when the ejectile emerges on the large-angle side of the momentum transfer vector, such that $\theta_p > \theta_q$. Hence, positive p_m for quasiperpendicular kinematics corresponds to an angle $\phi = 180°$ between the reaction and scattering planes.

V. CHANNEL COUPLING IN $^{12}C(e, e'N)$

A. Charge exchange for $T_0 = 70$ MeV

The role of charge exchange in neutron electromagnetic knockout was first investigated by van der Steenhoven et al. [60] using the Lane model. They predicted that the charge-exchange contribution to $(e, e'n)$ substantially increases the longitudinal response for that predominantly transverse reaction. For example, their calculations for $^{12}C(e, e'n)$ in parallel kinematics give as much as an order of magnitude enhancement of the neutron missing momentum distribution. However, Giusti and Pacati [58] found only very small effects using a similar model. On the other hand, using a con-
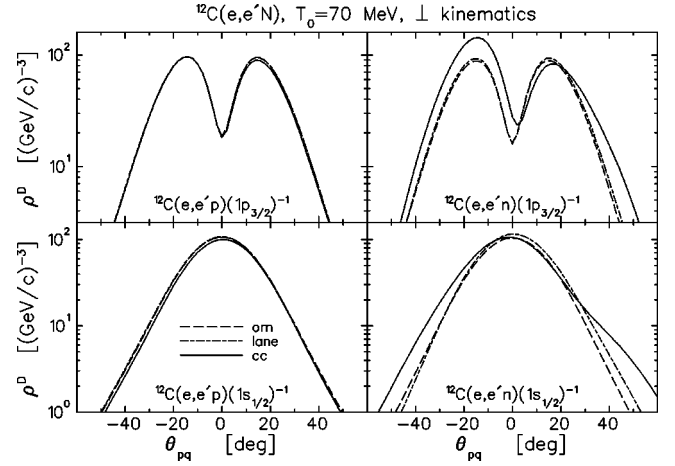

FIG. 1. Distorted momentum distributions for $^{12}C(e, e'N)$ in quasiperpendicular kinematics with $T_0 = 70$ MeV. Dashed curves show the optical model (OM), dash-dotted curves the Lane model, and solid curves the full coupled-channel calculation (CC). These calculations are normalized to full subshell occupancy.

tinuum RPA model, Jeschonnek et al. [12] obtained intermediate results which show much larger charge-exchange contributions than Giusti and Pacati that remain considerably smaller than those of van der Steenhoven et al. Their continuum RPA included coupling between states reached by both p-shell and s-shell knockout and employed a more complete model of final-state interactions that included spin-isospin components of the effective interaction.

We performed similar calculations for $^{12}C(e, e'N)$ using kinematics based upon the NIKHEF conditions. The electron beam energy was taken to be 461 MeV and all calculations maintain a constant total energy in the final state that is equivalent to a proton with 70 MeV kinetic energy incident upon the ground state of ^{11}B at rest. For simplicity we approximate the ground state using the independent-particle model, such that the model space consists of the four single-hole states reached by single-nucleon knockout. Coupling between these states is described by transition potentials obtained by folding the density-dependent Paris-Melbourne effective interaction for 65 MeV [53,54] with single-particle transition densities as described above.

Distorted momentum distributions for $1p_{3/2}$ and $1s_{1/2}$ knockout are shown for quasiperpendicular kinematics in Fig. 1 and for parallel kinematics in Fig. 2. These calculations are normalized to full subshell occupancy. We find that charge exchange within the Lane model has rather little effect, in qualitative agreement with Giusti and Pacati but in sharp disagreement with van der Steenhoven et al. Furthermore, the more complete model of channel coupling suggests very large contributions to $1p_{3/2}$ neutron knockout, in qualitative agreement with Jeschonnek et al., who do employ a more complete representation of the nucleon-nucleon interaction in the final state. The effects for proton knockout, especially for $1s_{1/2}$, are not entirely negligible either. These findings are independent of details of the kinematics, choice of optical potentials, or effective interactions, but are characteristic of the coupling schemes. The Lane model only couples analog states via spin-independent central potentials, whereas the dominant isospin-changing final-state interaction at these energies is $t_{\sigma\tau}$, which includes both spin and isospin
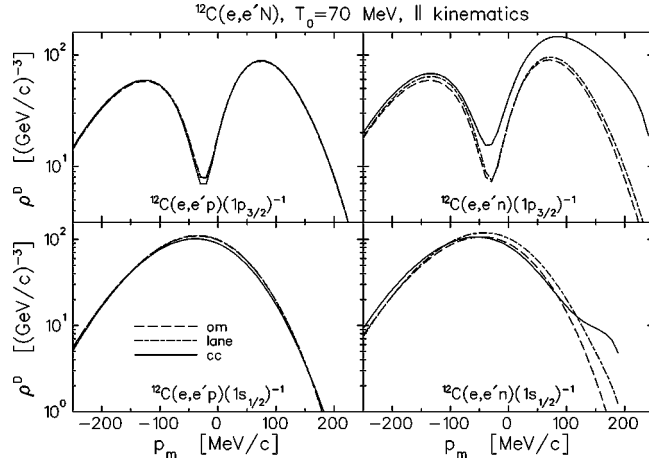
FIG. 2. Distorted momentum distributions for $^{12}C(e,e'N)$ in parallel kinematics with $T_0 = 70$ MeV. See Fig. 1 for legend.

transfer and tends to stimulate Gamow-Teller (GT) transitions. We also find that coupling to the $1s_{1/2}$ hole states is very important to $1p_{3/2}$ neutron knockout.

We also investigated the effect of expanding the model space to include $1p_{1/2}$ configurations. These states have relatively little effect upon the results shown here whether or not direct knockout from $1p_{1/2}$ orbitals is considered.

In Figs. 3–6 we show recoil polarizations for nucleon knockout at $T_0 = 70$ MeV expressed in the polarimeter basis. The greatest sensitivity to channel coupling is seen in P_y, which is independent of electron helicity and vanishes without FSI's. The effects of channel coupling are much larger for neutron knockout than for proton knockout, and much larger for the full model than for the Lane model used by Giusti and Pacati [58]. Note that without channel coupling

FIG. 4. Polarization of the recoil nucleon for $1s_{1/2}$ knockout in the $^{12}C(\vec{e},e'\vec{N})$ reaction using quasiperpendicular kinematics with $T_0 = 70$ MeV. See Fig. 3 for legend.

P_y for analog states reached by either neutron or proton knockout would be quite similar and that the isospin differences produced by the Lane potential are fairly small, but that the spin-isospin final-state interaction $t_{\sigma\tau}$ produces large differences between P_y for neutron and proton knockout.

The helicity-dependent polarization components P'_x and P'_z do not require FSI's and, hence, are less sensitive to channel coupling. We have also shown that these quantities are relatively insensitive to ambiguities in the single-nucleon
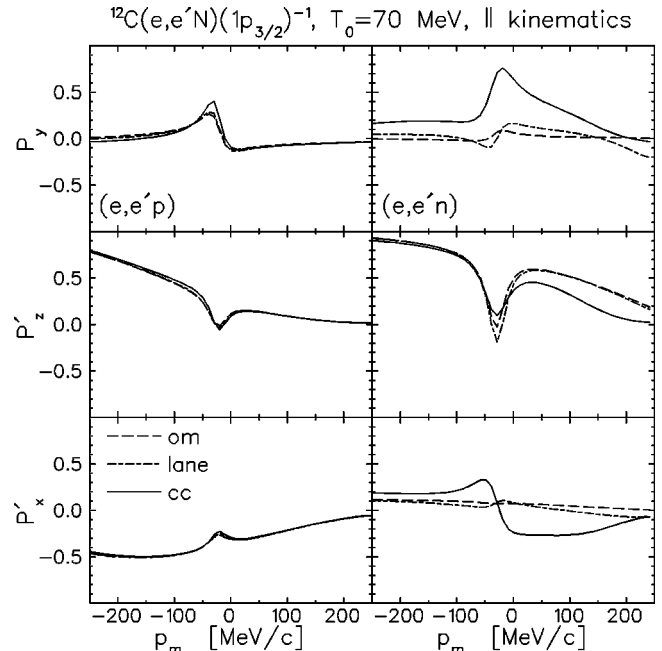

FIG. 3. Polarization of the recoil nucleon for $1p_{3/2}$ knockout in the $^{12}C(\vec{e},e'\vec{N})$ reaction using quasiperpendicular kinematics with $T_0 = 70$ MeV. Proton (neutron) knockout is shown in the left (right) column. See Fig. 1 for legend.

FIG. 5. Polarization of the recoil nucleon for $1p_{3/2}$ knockout in the $^{12}C(\vec{e},e'\vec{N})$ reaction using parallel kinematics with $T_0 = 70$ MeV. See Fig. 3 for legend.
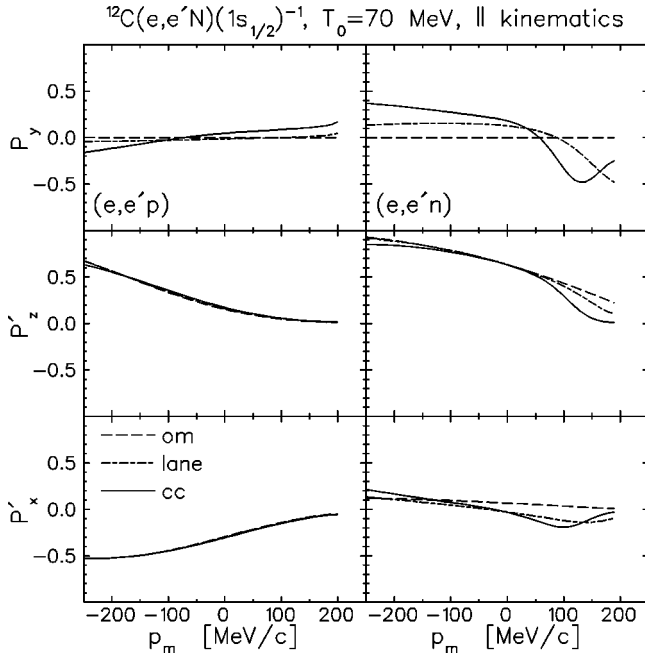
FIG. 6. Polarization of the recoil nucleon for $1s_{1/2}$ knockout in the $^{12}C(\vec{e},e'\vec{N})$ reaction using parallel kinematics with $T_0 = 70$ MeV. See Fig. 3 for legend.

current operator and to the choice of optical model [8]. Thus, it has been proposed that the ratio P'_x/P'_z is sensitive to the form factor ratio G_E/G_M in the nuclear medium. Figures 3–6 suggest that for proton knockout with modest missing momentum, channel coupling in FSI's should not complicate this analysis either, even for these rather low ejectile energies. (Nevertheless, two-body currents beyond the scope of the present investigation may play an important role.) However, for neutron knockout channel coupling does substantially affect the helicity-dependent recoil polarizations and, at least for this energy regime, would complicate similar attempts to deduce neutron form factors in the nuclear medium. With a more complete model of the final-state interactions, we obtain a much larger coupled-channel effect on polarization transfer for neutron knockout than calculated by Giusti and Pacati using the Lane model.

B. Induced polarization

The first measurements of the induced polarization P_N for a nucleus with $A > 2$ were made by Woo et al. [61] for $^{12}C(e,e'\vec{p})$ and the data for the $1p_{3/2}$ shell were found to be in good agreement with calculations based upon the distorted-wave impulse approximation (DWIA) using phenomenological optical potentials fitted to proton-scattering data. However, it is important to test whether channel coupling affects the induced polarization because P_N would vanish without FSI's. In Fig. 7 we compare calculations of the induced polarization for $^{12}C(e,e'\vec{p})$ with the recent data of Woo et al. [61] with $T_0 = 274$ MeV in quasiperpendicular kinematics. Final-state interactions were based upon the empirical effective interactions tabulated in Ref. [38], using linear interpolation with respect to energy. We find that channel coupling has very little effect upon the calculation for $1p_{3/2}$
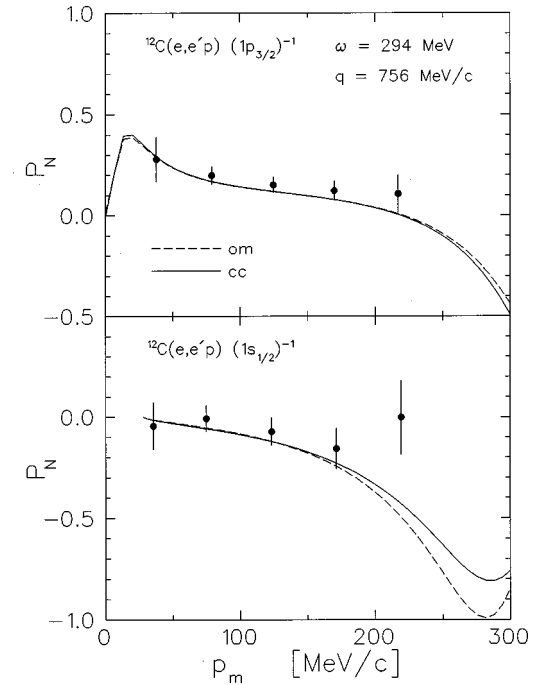

FIG. 7. Induced polarization of the recoil proton in the $^{12}C(e,e'\vec{p})$ reaction compared with the data of Woo et al. [61]. The data for the s shell are restricted to $28 < E_m < 39$ MeV to limit the contribution of the underlying continuum. Dashed curves show the optical model (OM) and solid curves show the full coupled-channel calculation (CC).

knockout, but is appreciable for $1s_{1/2}$ knockout when $p_m \gtrsim 200$ MeV/c; unfortunately, the data do not extend far enough to test that effect.

VI. CHANNEL COUPLING IN $^{16}O(\vec{e},e'\vec{N})$

A. Overlap functions

The overlap functions for p-shell proton knockout from ^{16}O were obtained from the $^{16}O(e,e'p)$ measurements of Leuschner et al. [62]. The data for parallel kinematics with $T_0 = 96$ MeV are compared with optical-model calculations using the Paris-Melbourne effective interaction in Fig. 8. Spectroscopic factors of 1.30 for $1p_{1/2}$ and 2.48 for $1p_{3/2}$ provide good visual fits to the data, but other choices of optical potential which also provide good descriptions of proton elastic scattering can give spectroscopic factors which differ by 10% or more [62,2]. Coupled-channel calculations are shown also, but deviations of a few percent are hardly visible on this scale. For the s-shell we used the parametrization of Elton and Swift [63]. For ^{15}O we used the same potential shapes and adjusted the central well depths to reproduce the separation energies for each state.

B. Channel coupling in $^{16}O(e,e'N)$ at $T_0 = 200$ MeV

We begin by considering the kinematics of MAMI experiment A1/2-93 [24], which will measure the $^{16}O(\vec{e},e'\vec{p})$ reaction using quasiperpendicular kinematics with $E_0 = 855$ MeV, $\omega = 215$ MeV, $q = 648$ MeV/c such that the ejectile energy is approximately 200 MeV. Measurements of
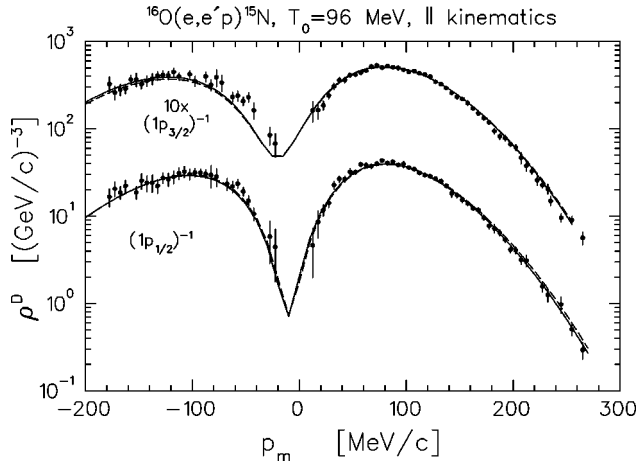
FIG. 8. Distorted momentum distributions for $^{16}O(e,e'p)$ in parallel kinematics with $T_0 = 96$ MeV. Spectroscopic factors of 1.30 for $1p_{1/2}$ and 2.48 for $1p_{3/2}$ are used to fit the calculations to the data of Leuschner *et al.* [62] for the dominant p-shell fragments. Dashed curves show the optical model (OM) and solid curves show the full coupled-channel calculation (CC).

all three components of the recoil polarization will be made with polarized beam on both sides of **q** in order to separate the even from the odd response functions. Thus, if statistics permit, it should be possible to separate R_{LT}, R_{LT}^N, $R_{LT}'^L$, $R_{TT}'^L$, $R_{LT}'^S$, and $R_{TT}'^S$ for several opening angles θ_{pq}. For completeness, we have also performed calculations for parallel kinematics using constant $T_0 = 200$ MeV.

Similar calculations for $T_0 = 135$ MeV were shown in Ref. [2]. Although the results are similar, the details depend upon ejectile energy. Furthermore, the calculations of Ref. [2] did not include $1s_{1/2}$ states in the model space, which we have since found to be important.
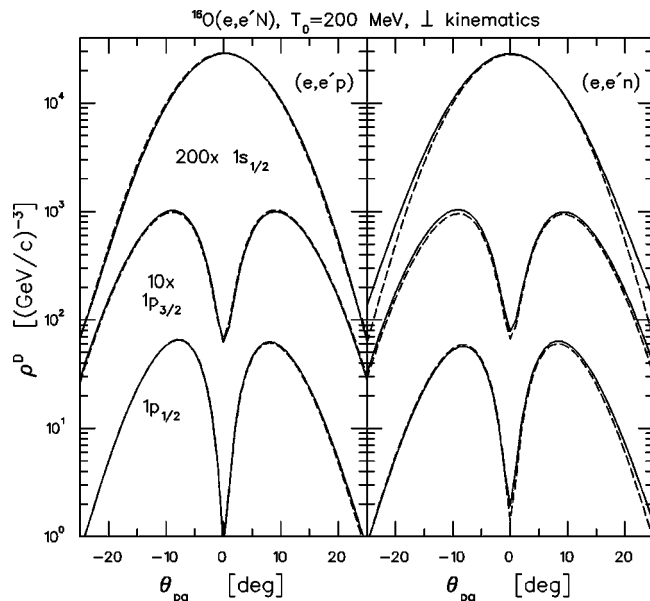
FIG. 9. Distorted momentum distributions for $^{16}O(e,e'N)$ in quasiperpendicular kinematics with $T_0 = 200$ MeV. Proton (neutron) knockout is shown on the left (right) side. These calculations are normalized to full subshell occupancy. See Fig. 8 for legend.
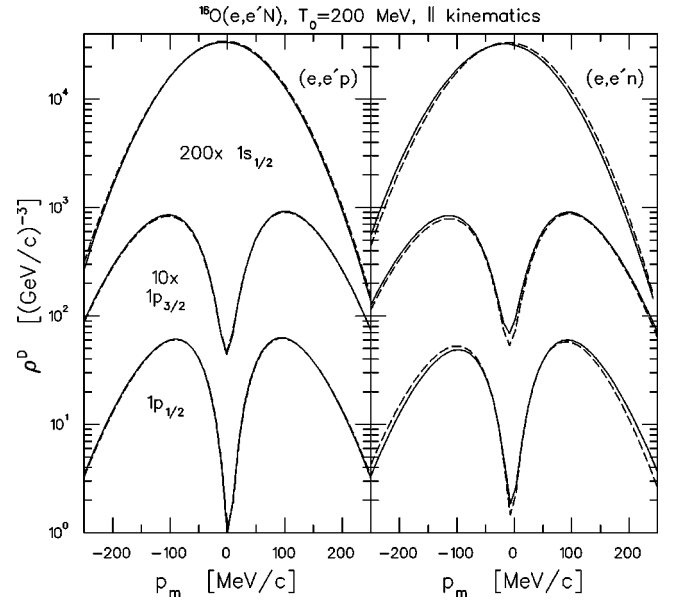

FIG. 10. Distorted momentum distributions for $^{16}O(e,e'N)$ in parallel kinematics with $T_0 = 200$ MeV. See Fig. 9 for legend.

1. Distorted momentum distributions

The reduced cross sections are shown in Fig. 9 for quasiperpendicular kinematics and in Fig. 10 for parallel kinematics. In addition, large missing momenta for quasiperpendicular kinematics with $\theta_p > \theta_q$ are shown in Fig. 11. These calculations are normalized to full subshell occupancy. The effect of channel coupling upon the reduced cross section for proton knockout appears to be quite small for $p_m \lesssim 300$ MeV/c, but can become appreciable for large p_m. At this energy channel coupling enhances the calculated cross section for p-shell proton knockout by factors of approximately 1.5–2 for $p_m \sim 500$ MeV/c and significantly alters the shape of the missing momentum distribution for $1s_{1/2}$ proton knockout. Similar calculations for $T_0 = 135$ MeV [2] show larger factors, especially for the $1p_{1/2}$ state, but details of these effects depend upon ejectile energy. Substantially larger enhancements of the cross section for $p_m > 300$ MeV/c were predicted for the rotational band in $^{10}B(e,e'p)^9Be$, with both reorientation and inelastic scatter-
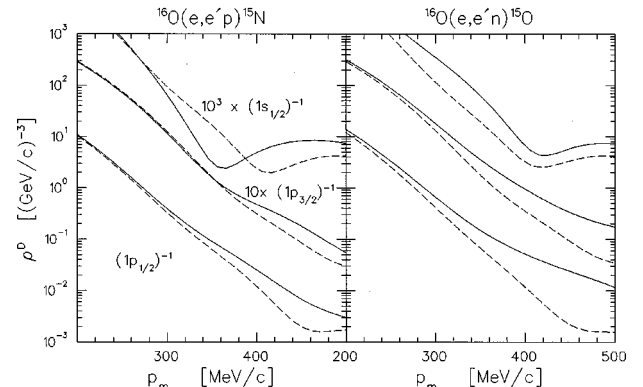

FIG. 11. Distorted momentum distributions for $^{16}O(e,e'N)$ in quasiperpendicular kinematics with $T_0 = 200$ MeV, selecting large missing momenta for $\theta_p > \theta_q$. See Fig. 9 for legend.
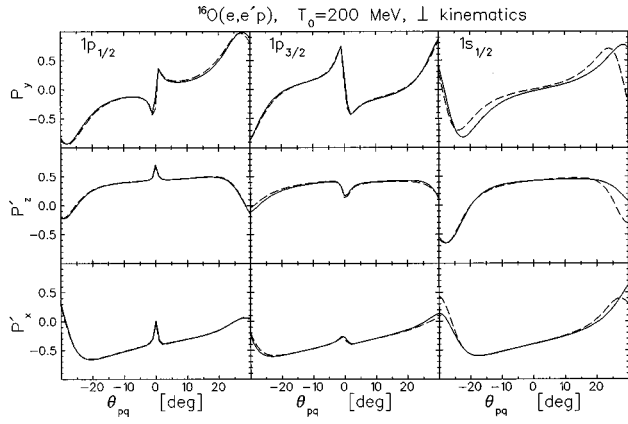
FIG. 12. Polarization of the recoil proton in the $^{16}O(\vec{e},e'\vec{p})^{15}N$ reaction using quasiperpendicular kinematics with $T_0 = 200$ MeV. The three columns show calculations for $1p_{1/2}, 1p_{3/2}$, and $1s_{1/2}$ knockout. Dashed curves show the optical model (OM) and solid curves show the full coupled-channel calculation (CC).

ing being equally important [22], because the quadrupole coupling is larger for that strongly deformed system. Hence, we conclude that the relative importance of various final-state interaction mechanisms depends upon nuclear structure in an essential manner. Furthermore, such effects will need to be examined carefully before any conclusions about high-momentum components due to short-range correlations are drawn from proton knockout data.

For $^{16}O(e,e'n)^{15}O$, channel coupling is significant even for p_m near the peaks of the momentum distributions. The most important couplings are those which change both the spin and the isospin of the residual nucleus. Although the effect on the cross section for quasiperpendicular kinematics is relatively small, changes in the left-right asymmetries for p-shell neutron knockout reflect substantial changes in the R_{LT} response functions that arise primarily from charge exchange in FSI's. Similarly, the modest enhancements of the cross section for neutron knockout in parallel kinematics originate in charge-exchange contributions to the longitudinal form factor. We also find that the missing momentum distributions for s-shell neutron knockout are broadened in quasiperpendicular and shifted in parallel kinematics by
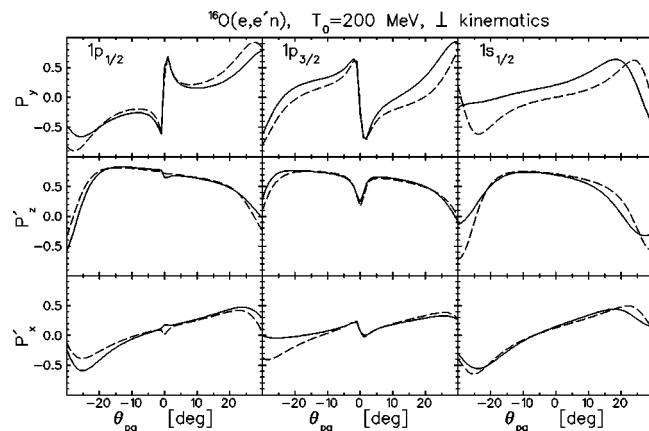

FIG. 14. Polarization of the recoil proton in the $^{16}O(\vec{e},e'\vec{p})^{15}N$ reaction using parallel kinematics with $T_0 = 200$ MeV. See Fig. 12 for legend.

charge exchange. For $p_m > 300$ MeV/c channel coupling enhances the cross section for neutron knockout by large factors relative to the conventional optical-model calculation. For $p_m \sim 500$ MeV/c and $T_0 = 200$ MeV, these factors approach an order of magnitude for p-shell neutron knockout with both charge exchange and inelastic scattering playing important roles. The effect of charge exchange upon neutron knockout was much larger at 70 MeV than it is at 200 MeV. Thus, we conclude that the importance of channel coupling decreases fairly rapidly as the ejectile energy increases, but for neutron knockout remains significant at 200 MeV.

2. Recoil polarization

Recoil-polarization observables expressed in the polarimeter basis are shown in Figs. 12 and 13 for quasiperpendicular kinematics and in Figs. 14 and 15 for parallel kinematics. For $p_m \lesssim 300$ MeV/c we find that channel coupling has practically no effect upon the polarization transfer for proton knockout. The effects of channel coupling upon the polarization transfer for neutron knockout are much smaller than at $T_0 = 70$ MeV, but remain non-negligible. Larger effects are obtained for $p_m \gtrsim 300$ MeV/c, but these variations remain comparable to those arising from ambiguities in the off-shell current operator explored in Ref. [8].

FIG. 13. Polarization of the recoil neutron in the $^{16}O(\vec{e},e'\vec{n})^{15}O$ reaction using quasiperpendicular kinematics with $T_0 = 200$ MeV. See Fig. 12 for legend.
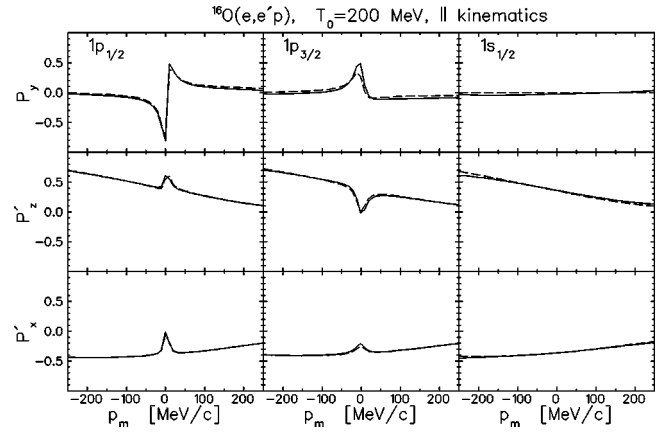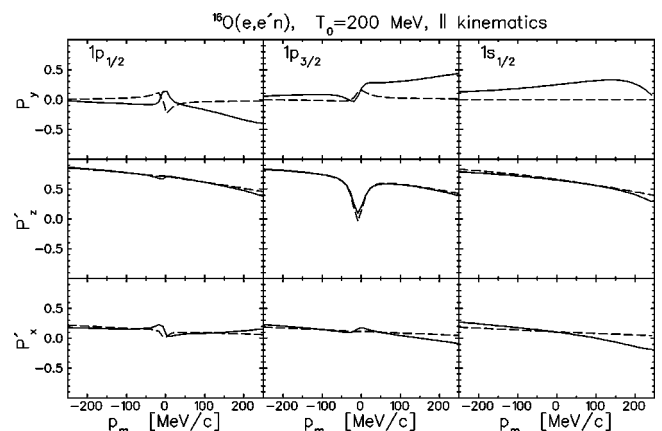

FIG. 15. Polarization of the recoil neutron in the $^{16}O(\vec{e},e'\vec{n})^{15}O$ reaction using parallel kinematics with $T_0 = 200$ MeV. See Fig. 12 for legend.
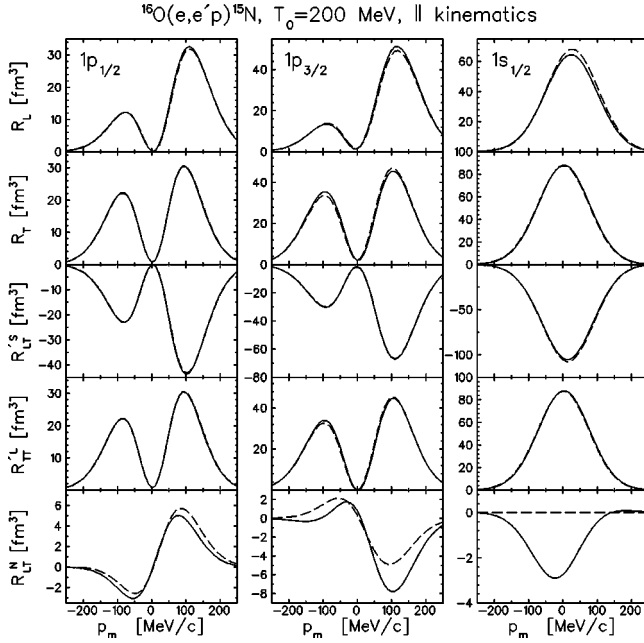
FIG. 16. Response functions for the $^{16}O(\vec{e},e'\vec{p})^{15}N$ reaction using parallel kinematics with $T_0 = 200$ MeV. These calculations are normalized to full subshell occupancy. See Fig. 12 for legend.

The induced polarization P_y is found to be more sensitive to channel coupling within final-state interactions. Small but non-negligible sensitivity to channel coupling in quasiperpendicular kinematics is exhibited by proton knockout, particularly for the s shell, whereas for neutron knockout channel coupling remains quite important even for modest missing momenta. The induced polarization for parallel kinematics is quite small for proton knockout, but for neutron knockout is substantially enhanced by channel coupling. We also find that channel coupling is generally more important than variations due to the choice of optical potential. Furthermore, although these effects decrease as T_0 increases from 135 to 200 MeV, the energy dependence is fairly slow.

It is interesting to note that P_y for s-shell knockout in parallel kinematics vanishes without channel coupling in the final state, but that a small polarization results from the spin dependence of channel coupling. The presence of an underlying continuum would make it difficult to observe this effect for $1s_{1/2}$ knockout, but it should be possible to observe this polarization for isolated s-shell knockout, such as $2s_{1/2}$ knockout from ^{40}Ca, given sufficient resolution.

3. Response functions

Response functions for parallel kinematics are shown in Fig. 16 for $^{16}O(\vec{e},e'\vec{p})^{15}N$ and in Fig. 17 for $^{16}O(\vec{e},e'\vec{n})^{15}O$. These calculations are normalized to full subshell occupancy. For proton knockout the largest effects are seen in R_{LT}^N, which vanishes without FSI's and for the s shell vanishes without channel coupling; hence, R_{LT}^N, which corresponds to P_N for parallel kinematics, tends to be most sensitive to details of the final-state interactions. For neutron knockout we find that charge exchange in the final state strongly enhances both R_L and R_{LT}^N and also has significant effects upon $R_{LT}^{'S}$, whereas the effects upon purely transverse response functions are much smaller.
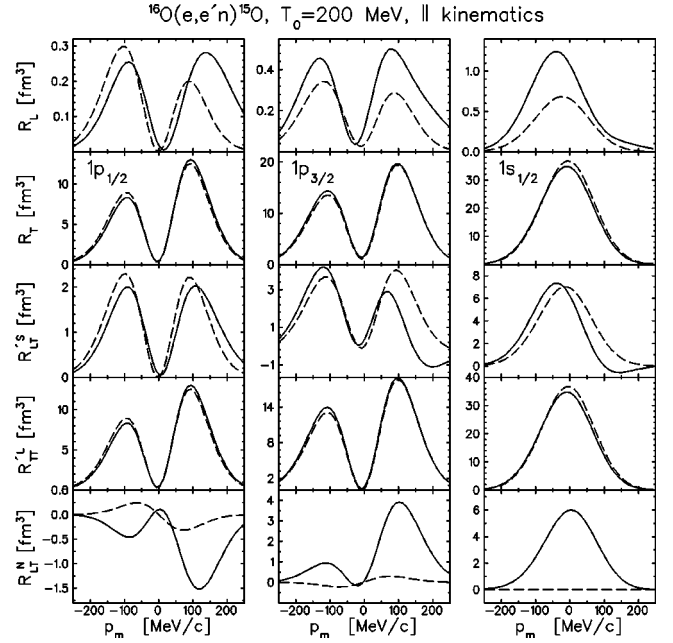

FIG. 17. Response functions for the $^{16}O(\vec{e},e'\vec{n})^{15}O$ reaction using parallel kinematics with $T_0 = 200$ MeV. See Fig. 16 for legend.

Selected response functions for coplanar quasiperpendicular kinematics are shown in Fig. 18 for $^{16}O(\vec{e},e'\vec{p})^{15}N$ and in Fig. 19 for $^{16}O(\vec{e},e'\vec{n})^{15}O$. We chose to show those response functions which potentially can be deduced from cross section and recoil polarization measurements on both sides of the momentum transfer vector for fixed electron-scattering kinematics because it is anticipated that MAMI
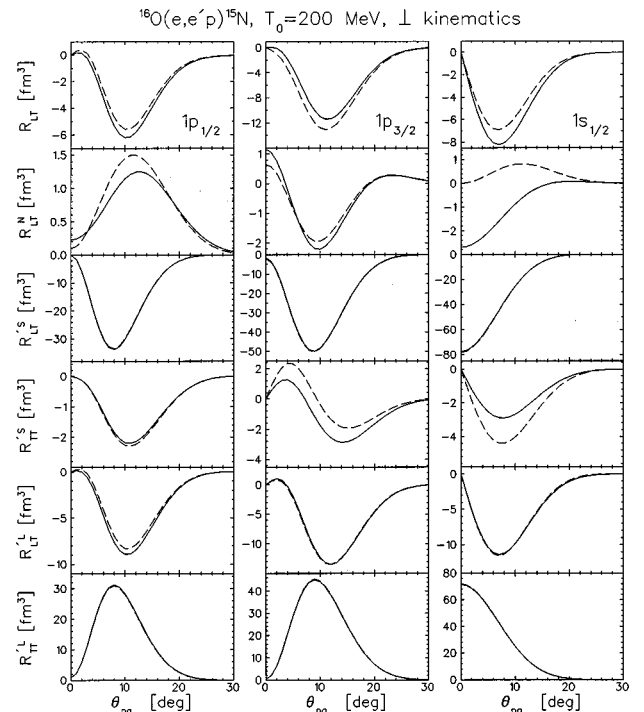

FIG. 18. Selected response functions for the $^{16}O(\vec{e},e'\vec{p})^{15}N$ reaction using coplanar quasiperpendicular kinematics with $T_0 = 200$ MeV. See Fig. 16 for legend.
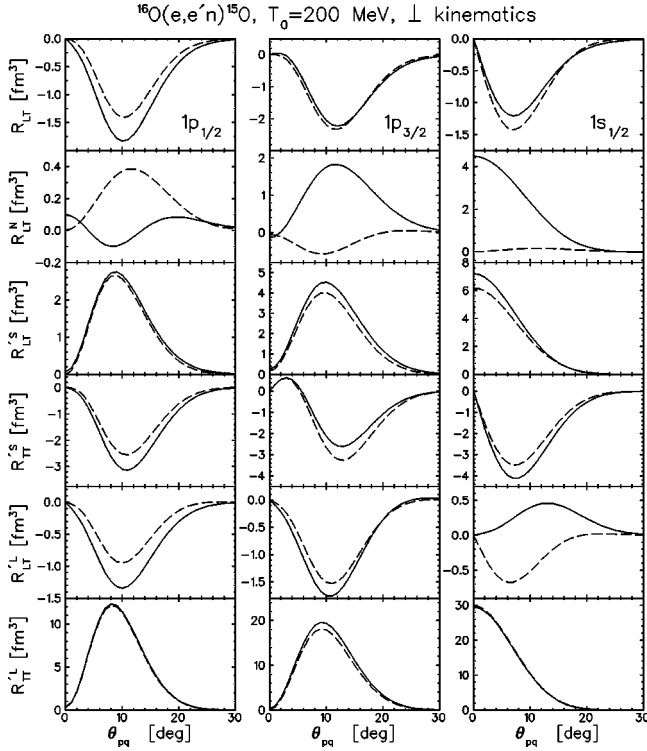
FIG. 19. Selected response functions for the $^{16}O(\vec{e},e'\vec{n})^{15}O$ reaction using coplanar quasiperpendicular kinematics with T_0 = 200 MeV. See Fig. 16 for legend.
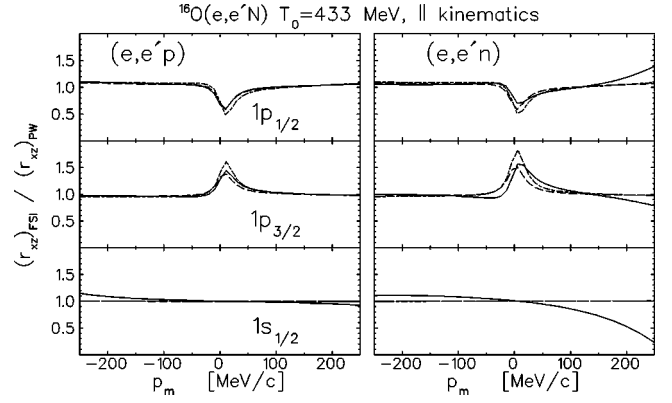

FIG. 20. The sensitivity of recoil polarization in parallel kinematics to FSI's is illustrated by comparing $r_{xz} = P'_x/P'_z$ to plane-wave (PW) calculations for the $^{16}O(\vec{e},e'\vec{N})$ reaction at T_0 = 433 MeV. The left (right) column shows proton (neutron) knockout and the three rows show calculations for $(1p_{1/2})^{-1}$, $(1p_{3/2})^{-1}$, and $(1s_{1/2})^{-1}$ final states. Dashed and dash-dotted curves represent EEI and EDAD1 optical-model calculations, while solid curves include channel coupling for EEI.

experiment A1/2-93 [24] will provide data of this type. The effects of channel coupling upon most strong class I response functions for proton knockout are relatively small, but at this energy remain appreciable for R_{LT} and R_{TT}. For p-shell proton knockout opposite effects upon R_{LT} are predicted for the two spin-orbit partners. There can also be significant effects upon some of the polarized class I response functions for proton knockout, such as $R_{TT}'^S$ for the $1p_{3/2}$ and $1s_{1/2}$ states. Therefore, the interpretation of response functions expected from MAMI experiment A1/2-93 [24] will need to consider channel coupling in the final state. The effects upon many of the class II response functions, such as R_{LT}^N, can be quite large even for proton knockout, especially for the $1s_{1/2}$ state. Note that without channel coupling, R_{LT}^m and R_{TT}^m with $m \in \{L,S\}$ would vanish for s-shell knockout, but those response functions become appreciable when spin-dependent channel coupling is present in the final state. Although not shown, strong modifications of R_{LT}^S, R_{LT}^L, and R_{TT}^L are predicted for p-shell proton knockout also.

Most class II response functions for neutron knockout are very strongly affected by channel coupling, with the most important channel couplings involving both isospin and angular momentum transfer. Although not shown in these figures, the Lane model produces much smaller effects because it lacks important spin-dependent and noncentral interactions. Unlike proton knockout, many of the class I response functions for neutron knockout also exhibit substantial sensitivity to channel coupling, especially the L- and LT-type response functions. Stronger effects were obtained in calculations for T_0 = 135 MeV where it was proposed to investigate the role of isobar currents in R_{LT} for $(e,e'n)$. Although the relative importance of channel coupling decreases as the

ejectile energy increases, these effects remain important at T_0 = 200 MeV. Therefore, it appears that it will be difficult to separate the effects of two-body currents from those of FSI's using neutron knockout at these energies. Perhaps higher ejectile energies will prove to be more favorable, but calculations including two-body currents are not available for larger Q^2.

C. Channel coupling in $^{16}O(\vec{e},e'\vec{N})$ at T_0 = 433 MeV

The first experiment to measure recoil polarization for polarized electron scattering from a target with $A > 2$ was performed recently at Jefferson Laboratory [25] and the data are presently being analyzed. The experiment used $^{16}O(\vec{e},e'\vec{p})$ in quasiperpendicular kinematics with E_0 = 2.445 GeV, ω = 0.445 GeV, and q = 1.0 GeV/c. Calculations for this reaction at T_0 = 433 MeV show that the effects of channel coupling on recoil polarization continue to decline as the ejectile energy increases; these effects are similar to but smaller than those shown for 200 MeV. Thus, it should be feasible to investigate possible medium modifications of the nucleon electromagnetic form factors for large Q^2 using quasifree recoil polarization.

A more quantitative assessment of the sensitivity of recoil polarization to various aspects of the model, including final-state interactions, can be made in terms of the polarization ratio

$$r_{xz} = P'_x/P'_z, \tag{51}$$

which for a free nucleon at rest is proportional to G_E/G_M [64]. We can then compare r_{xz} for a particular model either to a plane-wave calculation or to a baseline optical-model calculation.

In Figs. 20 and 21 we compare model calculations of the polarization ratio to their plane-wave limits for parallel and quasiperpendicular kinematics, respectively. FSI effects vary relatively slowly with missing momentum for $p_m \lesssim 250$ MeV/c, but the models quickly diverge from each
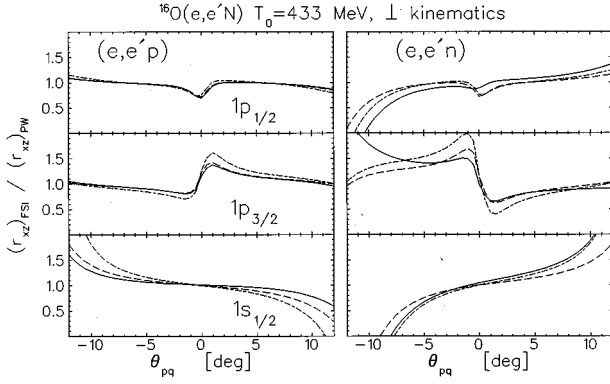
FIG. 21. The sensitivity of recoil polarization in quasiperpendicular kinematics to FSI's is illustrated by comparing $r_{xz} = P'_x/P'_z$ to plane-wave (PW) calculations for the $^{16}O(\vec{e},e'\vec{N})$ reaction at $T_0 = 433$ MeV. See Fig. 20 for legend.

other thereafter. Sensitivity to channel coupling in the final state is indicated by differences between dashed and solid curves, which are both based upon the EEI model but with the latter including channel coupling. Sensitivity to the choice of optical potential is indicated by the dashed and dash-dotted curves based upon the EEI and EDAD1 models, respectively. The EDAD1 potential is a global optical model fitted using Dirac phenomenology by Cooper *et al.* [65] to proton elastic-scattering data covering a wide range of energy and target mass, and represents a distinctly different approach than the EEI model. Also note that the IA2 interaction [38] gives results (not shown) that are practically indistinguishable from EEI over this range of p_m.

Figure 20 shows that final-state interactions have relatively little effect upon P'_x/P'_z for *p*-shell knockout in parallel kinematics except in the immediate vicinity of the node in the momentum distribution where the cross section becomes very small anyway. Not surprisingly, FSI corrections and model dependence are minimized near the peaks of the missing momentum distributions for each shell. Optical-model distortion for spin-orbit partners are opposite in direction and tend to balance for closed shells. Although *s*-shell knockout is insensitive to differences between optical models, the effects of channel coupling are somewhat larger than for the *p* shell. Nevertheless, these effects are minimal for $p_m = 0$ and nearly antisymmetric with respect to the sign of p_m for parallel kinematics. Therefore, it appears that when $Q^2 \gtrsim 0.5$ (GeV/c)^2 uncertainties in r_{xz} due to final-state interactions are only at the few percent level near the peaks of the missing momentum distributions for single-nucleon knockout in parallel kinematics.

Recoil-polarization ratios appear to be more sensitive for quasiperpendicular than for parallel kinematics to variations of the FSI model. The EDAD1 optical potential generally produces larger distortion corrections to these ratios than do either the EEI or IA2 potentials. The small differences between dashed and solid curves in Fig. 21 show that channel coupling has very little effect upon proton knockout from the *p* shell for modest opening angles, but the effects upon *p*-shell neutron knockout are substantially larger, especially on the beam side of the momentum transfer. FSI corrections to r_{xz} for *s*-shell knockout are relatively small for $\theta_{pq} \lesssim 5°$

where the cross section is fairly large, but become quite substantial for larger angles with small cross sections. (Note that when $p_m \approx 0$ at $\theta_{pq} = 0°$ for $1p_{1/2}$ in quasiperpendicular kinematics with $T_0 = 433$ MeV, then $p_m \approx 38$ MeV/c for $1s_{1/2}$ is signficantly larger.) Fortunately, FSI corrections are approximately antisymmetric with respect to **q** in quasiperpendicular kinematics, such that a symmetric acceptance would tend to reduce the net FSI effect and variations with respect to model. Furthermore, in parallel kinematics the FSI effects for spin-orbit partners also tend to compensate. Thus, the recoil-polarization ratio for inclusive quasifree knockout from a closed-shell nucleus centered upon $\mathbf{p}_m = 0$ is expected to be approximated well by a plane-wave calculation and small residual FSI corrections to not depend strongly upon model. Therefore, it appears that recoil polarization provides a nearly ideal probe of modifications of the electromagnetic current in nuclei for which uncertainties due to final-state interactions are relatively small.

Perhaps the simplest modification of the single-nucleon current would be a variation of nucleon electromagnetic form factors with density. Using the quark-meson coupling model, Thomas *et al.* [7] predict that for *p*-shell proton knockout from ^{16}O this ratio will be suppressed by about 10% relative to the free nucleon at $Q^2 = 0.8$ (GeV/c)^2. Similarly, Lu *et al.* [66] predict a 12% suppression of G_{En} in ^{3}He at $Q^2 = 0.5$ (GeV/c)^2. The present results suggest that final-state interactions will not obscure these medium modifications of nucleon form factors. This effect is predicted to increase with Q^2 and also becomes sensitive at large Q^2 to possible variation of the bag constant. An upcoming experiment [67] measuring recoil polarization for proton knockout from ^{4}He for several Q^2 between 0.8 and 4.0 (GeV/c)^2 should be sensitive to such variations of the bag model. However, two-body currents such as intermediate isobar excitation, relativistic distortion of nucleon spinors, or off-shell form factors may also affect the recoil-polarization ratio at the several percent level. Thus, because two-body currents are expected to affect neutron and proton knockout somewhat differently, it becomes important to perform measurements for both to distinguish between two-body contributions and modifications of the one-body current.

VII. SUMMARY AND CONCLUSIONS

We have developed a model of final-state interactions for $(\vec{e},e'\vec{N})$ reactions in which coupling between single-nucleon knockout channels is mediated by potentials obtained by folding density-dependent nucleon-nucleon effective interactions with nuclear transition densities using the local density approximation. Coupling to more complicated configurations is represented by optical potentials based upon the same effective interactions. All couplings within the model space and all components of the nucleon-nucleon interaction except tensor exchange are included. Hence, the model employs a more realistic description of final-state interactions and can be employed for higher energies than earlier models. Although the present applications use a one-body current operator and uncorrelated wave functions, the model can be extended to include two-body currents and ground-state correlations.

To compare our model of charge exchange FSI's with

earlier approaches, we analyzed the $^{12}C(\vec{e},e'\vec{N})$ reaction at $T_0 = 70$ MeV using a simple four-state coupling scheme based upon pure $1p_{3/2}$ and $1s_{1/2}$ hole states. Although van der Steenhoven *et al.* [60] predicted strong charge-exchange contributions to $(e,e'n)$ under these conditions using the Lane model, we obtain rather small effects for this model, in agreement with Giusti and Pacati [58]. However, strong charge-exchange contributions to the $(e,e'n)$ cross section are obtained when the $t_{\sigma\tau}$ final-state interaction is included. Similar findings were also obtained by Jeschonnek *et al.* [12]. We also find that recoil polarization for $(\vec{e},e'\vec{n})$ is quite sensitive to channel coupling, including the helicity-dependent components, while $(\vec{e},e'\vec{p})$ remains rather insensitive to these complications even for these relatively low ejectile energies.

We studied the $^{16}O(\vec{e},e'\vec{N})$ reactions at $T_0 = 200$ and 433 MeV, kinematics appropriate to experiments at MAMI and TJNAF, using a six-state coupling scheme based upon the independent-particle model. We find that channel coupling has very little effect upon the proton knockout cross section for missing momenta $p_m < 300$ MeV/c and that the charge-exchange contribution to neutron knockout decreases as the ejectile energy increases, but that channel coupling remains important for neutron knockout at $T_0 = 200$ MeV. For larger p_m channel coupling has important effects upon the cross sections for both proton and neutron knockout even when $T_0 = 433$ MeV and these effects depend strongly upon both nuclear structure and kinematics.

Most of the response functions for proton knockout that would remain finite in the absence of FSI's appear to be relatively insensitive to channel coupling, but response functions for neutron knockout, especially those which vanish without FSI's, are considerably more sensitive to channel coupling. Charge exchange mediated by the $t_{\sigma\tau}$ interaction is the most important coupling mechanism for $^{16}O(\vec{e},e'\vec{N})$, but quadrupole inelastic scattering can be important also for deformed targets.

The polarization transfer observables P'_S and P'_L for proton knockout with modest missing momentum appear to be quite insensitive to details of the final-state interaction, including channel coupling. Although the corresponding quantities for neutron knockout are affected at low energies by channel coupling, these effects decrease with energy and become relatively small for $T_0 = 433$ MeV. FSI model dependence is minimized for parallel kinematics near peaks of the missing momentum distributions for each shell or for inclusive quasifree knockout with momentum acceptance that is symmetric about $\mathbf{p}_m = 0$. Furthermore, these quantities appear to be insensitive to ambiguities in gauge or off-shell properties of the one-body electromagnetic current operator. Hence, recoil polarization provides an ideal means for investigating the electromagnetic current in the nuclear medium. To the extent that the one-body current is dominant, the simple relationship between P'_S/P'_L and G_E/G_M provides a means for studying possible density dependence of nucleon electromagnetic form factors. However, the role of two-body currents at high Q^2 has not yet been investigated and may be important also. Therefore, it is important to measure separated response functions which will provide differing sensitivities to these two mechanisms.

The present formalism would permit many technical improvements to be implemented in a relatively straightforward manner, including correlated wave functions, expanded model spaces, improved electron distortion and initial-state coupling, and nonlocal final-state interactions. Extension to relativistic FSI models is also possible. However, perhaps the most interesting extensions involve the effective current operator. In addition to conventional two-body currents, the quark-meson coupling model suggests that nucleon electromagnetic form factors are density dependent. The implications of density-dependent form factors can be investigated by applying the local density approximation to the one-body current operator. The present results suggest that these effects, and those of two-body currents, can be studied with relatively little uncertainty due to final-state interactions using recoil polarization for energetic ejectiles.

[1] A.E.L. Dieperink and P.K.A. de Witt Huberts, Annu. Rev. Nucl. Part. Sci. **40**, 239 (1990).

[2] J.J. Kelly, Adv. Nucl. Phys. **23**, 75 (1996).

[3] S. Boffi, C. Giusti, and F.D. Pacati, Phys. Rep. **226**, 1 (1993).

[4] S. Boffi, C. Giusti, F. D. Pacati, and M. Radici, *Electromagnetic Response of Atomic Nuclei* (Oxford University Press, Oxford, 1996).

[5] D.H. Lu, A.W. Thomas, K. Tsushima, and A.G. Williams, Phys. Lett. B **417**, 217 (1998).

[6] D.H. Lu, K. Tsushima, A.W. Thomas, and A.G. Williams, Nucl. Phys. **A634**, 443 (1998).

[7] A.W. Thomas, D.H. Lu, K. Tsushima, and A.G. Williams, "Recent results from QMC relevant to TJNAF," nucl-th/9807027, 1998.

[8] J.J. Kelly, Phys. Rev. C **56**, 2672 (1997).

[9] J. Ryckebusch, K. Heyde, D. van Neck, and M. Waroquier, Nucl. Phys. **A503**, 694 (1989).

[10] J. Ryckebusch, M. Waroquier, K. Heyde, J. Moreau, and D. Ryckbosch, Nucl. Phys. **A476**, 237 (1988).

[11] V. van der Sluys, J. Ryckebusch, and M. Waroquier, Phys. Rev. C **54**, 1322 (1996).

[12] S. Jeschonnek, A. Szczurek, G. Co, and S. Krewald, Nucl. Phys. **A570**, 599 (1994).

[13] K. Nakayama, S. Krewald, J. Speth, and W.G. Love, Nucl. Phys. **A431**, 419 (1984).

[14] M.A. Franey and W.G. Love, Phys. Rev. C **31**, 488 (1985).

[15] J.J. Kelly, Phys. Rev. C **39**, 2120 (1989).

[16] H. Seifert *et al.*, Phys. Rev. C **47**, 1615 (1993).

[17] J.J. Kelly *et al.*, Phys. Rev. C **43**, 1272 (1991).

[18] B.S. Flanders *et al.*, Phys. Rev. C **43**, 2103 (1991).

[19] J.J. Kelly *et al.*, Phys. Rev. C **44**, 2602 (1991).

[20] J.J. Kelly, Phys. Rev. C **54**, 2547 (1996).

[21] J.J. Kelly, Phys. Rev. C **46**, 711 (1992).

[22] L.J. de Bever *et al.*, Nucl. Phys. **A579**, 13 (1994).

[23] J.J. Kelly, in *Proceedings of the Second Workshop on Electromagnetically Induced Two-Nucleon Knockout*, edited by J. Ryckebusch and M. Waroquier (UE Press, Gent, 1995), pp. 269–274.

[24] R. Neuhausen *et al.*, Measurement of Polarized Protons from Quasielastic Electron Scattering on ^{16}O, MAMI Proposal No. A1/2-93, 1993.

[25] C. Glashausser *et al.*, Measurement of Recoil Polarization in the ^{16}O$(e,e'p)$ Reaction with 4 GeV Electrons, TJNAF Proposal No. 89-033, 1989.

[26] G. Rawitscher, Phys. Rev. C **56**, 2029 (1997).

[27] R.L. Mercer, Phys. Rev. C **15**, 1786 (1977).

[28] S. Boffi, C. Giusti, F.D. Pacati, and S. Frullani, Nucl. Phys. **A319**, 461 (1979).

[29] Y. Jin, H.P. Blok, and L. Lapikás, Phys. Rev. C **48**, R964 (1993).

[30] V. van der Sluys, K. Heyde, J. Ryckebusch, and M. Waroquier, Phys. Rev. C **55**, 1982 (1997).

[31] L.L. Schiff, Phys. Rev. **103**, 443 (1956).

[32] K.S. Kim and L.E. Wright, Phys. Rev. C **56**, 302 (1997).

[33] H. Feshbach, *Theoretical Nuclear Physics: Nuclear Reactions* (Wiley, New York, 1992).

[34] L. Ray, G.W. Hoffmann, and W.R. Coker, Phys. Rep. **212**, 223 (1992).

[35] L. Kurth, B.C. Clark, E.D. Cooper, S. Hama, S. Shim, R.L. Mercer, L. Ray, and G.W. Hoffmann, Phys. Rev. C **49**, 2086 (1994).

[36] V.K. Mishra, B.C. Clark, E.D. Cooper, and R.L. Mercer, Phys. Rev. C **41**, 370 (1990).

[37] R.J. Furnstahl and S.J. Wallace, Phys. Rev. C **47**, 2812 (1993).

[38] J.J. Kelly and S.J. Wallace, Phys. Rev. C **49**, 1315 (1994).

[39] S. Boffi, F. Cannata, C. Giusti, and F.D. Pacati, Nucl. Phys. **A379**, 509 (1982).

[40] T. de Forest, Nucl. Phys. **A392**, 232 (1983).

[41] M.F. Gari and W. Krümpelmann, Phys. Lett. B **274**, 159 (1992).

[42] M.F. Gari and W. Krümpelmann, Phys. Lett. B **282**, 483 (1992).

[43] S. Frullani and J. Mougey, in *Advances in Nuclear Physics*, edited by J.W. Negele and E. Vogt (Plenum Press, New York, 1984), Vol. 14.

[44] H.W.L. Naus, S.J. Pollock, J.H. Koch, and U. Oelfke, Nucl. Phys. **A509**, 717 (1990).

[45] X. Song, J.P. Chen, P.K. Kabir, and J.S. McCarthy, J. Phys. G **17**, L75 (1991).

[46] C.R. Chinn and A. Picklesimer, Nuovo Cimento A **105**, 1149 (1992).

[47] W.T. Pinkston and G.R. Satchler, Nucl. Phys. **72**, 641 (1965).

[48] H.P. Blok and G. van der Steenhoven, Phys. Rev. C **35**, 2347 (1987).

[49] J. Raynal, Technical Report No. IAEA-SMR-9/8, Centre d'études Nucléaires de Saclay (unpublished).

[50] J.J. Kelly, program manual for LEA (unpublished).

[51] J.J. Kelly *et al.*, Phys. Rev. Lett. **45**, 2012 (1980).

[52] J.J. Kelly *et al.*, Phys. Rev. C **39**, 1222 (1989).

[53] P.J. Dortmans and K. Amos, Phys. Rev. C **49**, 1309 (1994).

[54] S. Karataglidis, P.J. Dortmans, K. Amos, and R. de Swiniarski, Phys. Rev. C **52**, 861 (1995).

[55] T. Cheon, K. Takayanagi, and K. Yazaki, Nucl. Phys. **A437**, 301 (1985).

[56] T. Cheon, K. Takayanagi, and K. Yazaki, Nucl. Phys. **A445**, 227 (1985).

[57] T. Cheon and K. Takayanagi, Phys. Rev. Lett. **68**, 1291 (1992).

[58] C. Giusti and F.D. Pacati, Nucl. Phys. **A504**, 685 (1989).

[59] A. Picklesimer and J.W. van Orden, Phys. Rev. C **40**, 290 (1989).

[60] G. van der Steenhoven, H.P. Blok, M. Thies, and P.J. Mulders, Phys. Lett. B **191**, 227 (1987).

[61] R.J. Woo *et al.*, Phys. Rev. Lett. **80**, 456 (1998).

[62] M. Leuschner *et al.*, Phys. Rev. C **49**, 955 (1994).

[63] L.R.B. Elton and A. Swift, Nucl. Phys. **A94**, 52 (1967).

[64] R.G. Arnold, C.E. Carlson, and F. Gross, Phys. Rev. C **23**, 363 (1981).

[65] E.D. Cooper, S. Hama, B.C. Clark, and R.L. Mercer, Phys. Rev. C **47**, 297 (1993).

[66] D. Lu, K. Tsushima, A.W. Thomas, and A.G. Williams, Phys. Lett. B **441**, 27 (1998).

[67] J.F.J. van den Brand *et al.*, Polarization Transfer in the Reaction ^{4}He$(\vec{e},e'\vec{p})$ in the Quasi-elastic Scattering Region, TJNAF Proposal No. 93-049, 1993.